A STUDY OF THE INTRODUCTION OF IONS INTO THE REGION OF STRONG FIELDS WITHIN A QUADRUPOLE MASS SPECTROMETER

By
WILSON M. BRUBAKER

BELL & HOWELL RESEARCH CENTER
360 SIERRA MADRE VILLA
PASADENA, CALIFORNIA

CONTRACT NASW-1298

QUARTERLY PROGRESS REPORT
for the period
17 AUGUST 1965 TO 17 NOVEMBER 1965

NATIONAL AERONAUTICS AND SPACE ADMINISTRATION
WASHINGTON, D.C.

A STUDY OF THE INTRODUCTION OF IONS INTO THE REGION OF STRONG FIELDS WITHIN A QUADRUPOLE MASS SPECTROMETER

By
WILSON M. BRUBAKER

BELL & HOWELL RESEARCH CENTER
360 SIERRA MADRE VILLA
PASADENA, CALIFORNIA

CONTRACT NASW-1298

QUARTERLY PROGRESS REPORT
for the period
17 AUGUST 1965 TO 17 NOVEMBER 1965

NATIONAL AERONAUTICS AND SPACE ADMINISTRATION
WASHINGTON, D.C.

A STUDY OF THE INTRODUCTION OF IONS INTO THE REGION OF STRONG FIELDS WITHIN A QUADRUPOLE MASS SPECTROMETER

by

Wilson M. Brubaker

ABSTRACT

19583

This project is a theoretical and experimental study of the introduction of ions into the strong fields of a quadrupole mass filter. Theoretical studies only have been made during the first quarter, although experimental apparatus have been assembled. These studies consist of computer-calculated trajectories of ions, including their passage through the fringing fields, where the field intensities grow from zero to full value. It is found that that the maximum amplitudes of the ions as they traverse the filter are strongly dependent upon the assumed spatial distribution of the fringing fields. For the conventional quadrupole, operated at high resolving power, it is found that the transmission efficiency is extremely low, because only those ions which enter the quadrupole under nearly ideal conditions (on the axis and parallel to it) have trajectory amplitudes less than the distance to the rods. If, through the use of a second set of four electrodes, the dc component of the field is delayed relative to the ac component in the fringe region, the transmission efficiency is greatly increased.

Author.

TABLE OF CONTENTS

LIST OF FIGURES IN TEXT

LIST OF FIGURES IN APPENDIX

Figure

INTRODUCTION

This is the first quarterly report of the work done by the Bell & Howell Research Center on NASA Contract NASW-1298. It covers the period from the initiation of the contract, August 17, 1965, through November 17, 1965.

This project is concerned initially with the introduction of ions into the region of strong fields within a quadrupole mass filter. Since it is usually impossible or impractical to form the ions within the strong field region of the mass filter, they are normally formed outside the filter, where the quadrupole fields are essentially zero. As the ions traverse the region of fringing fields (defined as the space which is bounded on one side by nearly zero quadrupole fields, and on the other by the full field of the mass filter), they are subjected to accelerations which grossly alter their trajectories. These alterations usually are very detrimental in that they greatly diminish the probability of the ion traversing the filter without striking the rods.

That the traversal of the fringing fields results in these undesirable consequences has been recognized for years; but without the services of a digital computer, it has been impossible to evaluate the effect. The use of a computer in these studies has dramatically shown the seriousness of this effect in the usual quadrupole geometry. It has also shown that a proposed solution to this problem appears to be practical.

A part of this project includes the investigation of the deterioration of the performance of the quadrupole which results from the use of round, rather than hyperbolic, field-forming surfaces. All of the theories of the quadrupole have assumed that the surfaces are hyperbolic, when in reality almost all quadrupoles have been constructed with round cylinders, normally called "rods." However, the theoretical considerations given here are based on the assumption of hyperbolic surfaces. The study of the performance degradation caused by the use of round rods will be made later.

THEORY

General Theory

A schematic of a laboratory quadrupole, using round rods, and the manner of excitation is shown in Fig. 1. When round rods are used, their radius is made slightly larger than the instrument radius, r_o, to better approximate the hyperbolic fields with circular-shaped electrodes.

The formal, classical, exact theory of the motion of the ions as they traverse the quadrupole is given by the Mathieu equation. It is revealed by the solutions of the Mathieu euqation that the amplitudes of the trajectories are either stable, or unstable. That is, they oscillate between bounded limits, or they grow without limit with time. This portion of the Mathieu solution is applied directly, and simply to the problem.

The derivation of the actual trajectories from the Mathieu equation is a most laborious job, and is not attempted in this report. However, the solutions of the Mathieu equation are given, in their infinite series form, for identification.

A simplified, approximate theory of the y-component of the motion of the ions in the quadrupole field was presented at the meeting of the American Physical Society in 1961. The appropriate parts of this theory are presented in this report, as they are necessary to give a basis for the understanding of the physics of the ionic motions.

This theory may be referred to in later quarterly reports, but it will not be repeated until the preparation of the final report.

Formal Theory

The formal theory of the quadrupole mass filter[1] is based upon the use of field-forming surfaces which are hyperbolic cylinders. For use of the quadrupole in the laboratory, it has been found that the compromise of using round rods instead of the hyperbolic cylinders is an expedient one to make.

---

1. Paul, W.; Reinhard, H. P.; and von Zahn, U.: Z. Physik, vol. 152, 1958, p. 143.

For space applications, where power and performance must be optimized, this may be a poor compromise. Later in this project an attempt will be made to evaluate the sacrifice in performance which this compromise causes.

When hyperbolic surfaces are used, the potential throughout the space between the field-forming surfaces is given by:

$$V = (V_{dc} + V_{ac} \cos \omega t)\ (x^2 - y^2)/r_o^2. \tag{1}$$

The gradients are given by:

$$E_x = (V_{dc} + V_{ac} \cos \omega t)\ (-2x/r_o^2), \tag{2}$$

and,

$$E_y = (V_{dc} + V_{ac} \cos \omega t)\ (+2y/r_o^2). \tag{3}$$

Note that the x-component of gradient is independent of the y-variable and vice versa. Because the x-component of motion is completely independent of the y-position, the motions in the x - z plane can be considered entirely independently of the motions in the y - z plane and vice versa.

The equations of motion of the ions are obtained by the integration of the force equations. In this case, the integration cannot be done directly or simply. The equations are:

$$M\ddot{x} = eE_x = -(2e/r_o^2)\ (V_{dc} + V_{ac} \cos \omega t)\ x, \tag{4}$$

$$M\ddot{y} = eE_y = +(2e/r_o^2)\ (V_{dc} + V_{ac} \cos \omega t)\ y. \tag{5}$$

Equations (4) and (5) are transformed to the standard Mathieu equation through the use of the dimensionless variables a, q and τ. The transformations which accomplish this are:

$$a = 8eV_{dc}/Mr_o^2\omega^2,$$

$$q = 4eV_{ac}/Mr_o^2\omega^2,$$

$$\tau = \frac{\omega t}{2}.$$

The transformed equations are:

$$\frac{d^2x}{d\tau^2} + (a + 2q \cos 2\tau)\ x = 0, \tag{6}$$

$$\frac{d^2y}{d\tau^2} - (a + 2q \cos 2\tau) y = 0 . \qquad (7)$$

The solutions of the Mathieu equation are given in books by McLachlan,[2] and by Meixner and Schafke.[3]

They are characterized by regions of stability and regions of instability. The amplitude of the variable (x or y) remains bounded in the former case, and increases without limit in the latter. Whether the trajectory is stable or unstable is determined solely by the values of a and q. The a, q plane is divided into stable and unstable regions as shown in Fig. 2. The region of interest for the mass filter is limited to values of a and q less than unity. An enlarged view of this portion is shown in Fig. 3.

In order for ions which are incident upon the filter with random components of radial velocity to traverse the filter and reach the collector, their trajectories must be stable for both the x- and y-components of velocity. Further, their amplitudes must be less than r_o. Reference to Eqs. (6) and (7) shows that the only difference between the force equation for the x- and y-components of motion is the sign of the coefficients of a and q. By reflecting the stability criteria for the negative or y equation about the line a = 0, the stability criteria are superimposed. The results are shown in Figure 4.

For a given ratio of the dc voltage to the ac voltage, all values of a and q lie on the scan line which passes through the origin. Each point on this line corresponds to a value of mass-to-charge ratio of the (m/e) of the ion. The interval of this value, d(m/e), which lies within the stability diagram, corresponds to the range of masses whose trajectories are stable. If the ratio of the dc to the ac voltage is increased, the slope of the scan line is increased, and it passes nearer to the apex of the stability diagram. This causes the interval dm/m to decrease and the resolving power m/dm to increase. By changing the ratio of (V_{ac} and V_{dc})/ω^2, ions of any chosen m/e ratio can be caused to have stable trajectories.

A mass scan is accomplished by varying the ratio of the applied voltages to the frequency. Usually the voltages are varied but mass spectrometers have been constructed in which the frequency is varied to produce a mass scan.

---

2. McLachlan: Theory and Application of Mathieu Functions, (Oxford), 1947.

3. Meixner, J.; and Schafke, F. W.: Mathieusche Funktionen und Spharioid-funktionen. (Berlin), 1954.

Reference to Fig. 4 shows that the portions of the a, q diagram for which the solutions are stable is limited to values of β which lie between 0 and 1. The general solution which describes the amplitude of the trajectory as a function of time is given by McLachlan as

$$y(\tau) = A \sum_{r=-\infty}^{r=+\infty} c_{2r} \cos(2r + \beta)\tau + B \sum_{r=-\infty}^{r=+\infty} c_{2r} \sin(2r + \beta)\tau \qquad (8)$$

The coefficients of the terms of the infinite series are themselves continued fractions. Further, there is no simple relationship between the known variables a and q and the dependent variable β which appears in the above equation.

Approximate Solutions, Based upon Physical Principles

Equations (4) and (5) for the x- and y-components of force differ only by a minus sign. For the steady state conditions, this has no significance for the ac term, as it merely represents a phase shift of 180°. Hence the difference between the motions in the x - z and y - z planes results solely from the influence of the dc term. In particular, when the dc component of the field is zero, strong focusing results. This is the principle upon which many modern particle accelerators operate. It is also denoted as alternating gradient focusing.

The influence of the dc field is to render the trajectories unstable. Reference to Fig. 4 shows that relatively small amounts of dc potential as contained in the dimensionless variable a, suffice to render the y-component of the trajectories unstable even in the presence of sizeable quantities of ac fields. In contrast, it is noted that the addition of small amounts of dc field superimposed upon large amounts of ac field have minor effects on the stability of the x-component of motion.

It is of interest to consider the mechanism whereby the dc gradient causes the trajectories to be unstable. Reference to Eq. (4) shows that the x-component of motion is stable under the influence of dc potentials only. In the absence of ac potentials the ions execute simple harmonic motion at a resonant frequency. Energy can be stored in a resonant system and so the fact that the addition of the appropriate amounts of ac fields renders the trajectory unstable is not surprising. Reference to Eq. (5) shows that under the influence of dc fields only, the y-component of motion is unstable; the acceleration is proportional to y and is directed away

from the axis. The problem here is to show how the trajectories can be made stable in the presence of dc fields by the addition of much stronger ac fields.

Approximate Solutions, the Y-Component of Motion

Equation (5) shows that the dc field accelerates a positive ion away from the axis. If stability is to be obtained, it must result from the interaction of the ion and the ac field. An analysis of the motion of the ion in response to the alternating electric field whose strength is proportional to the distance from the axis leads to an evaluation of this interaction. The boundary between the stable and the unstable portions of the stability diagram is characterized by a balance between the inwardly-directed acceleration due to this interaction and the outwardly-directed acceleration in the dc field. For other a, q values, these accelerations are not balanced. In the unstable portion the dc-derived acceleration dominates and the trajectory expands without limit. In the stable portion the ac-derived acceleration dominates, and the average position of the ion oscillates slowly with bounded amplitude about the x-z plane.

The acceleration in the dc field is obtained by setting $q = 0$ in Eq. (5),

$$\ddot{y}_{dc} = (2eV_{dc}/Mr_o^2)\, y$$

$$= (a/4)\, \omega^2 y \,. \tag{9}$$

The average acceleration owing to the interaction with the ac fields is obtained in an approximate manner. It is assumed that the ion is oscillating in response to the ac field, at an average position $\bar{y}$. Any drift velocity is assumed to be negligible relative to the velocity of oscillation. As a first approximation, the space-dependence of the field is ignored. This gives sinusoidal motion. Setting $a = 0$ in Eq. (5) and normalizing to the dimensionless variable q,

$$\frac{d^2y}{dt^2} = (1/2)\, q\omega^2\bar{y} \cos \omega t. \tag{10}$$

Integrating and using the boundary conditions yields

$$y = \bar{y} \left[1 - (1/2)q \cos \omega t \right] . \tag{11}$$

The value of q in the vicinity of the apex of the stability triangle is 0.7. For a, q values near the apex,

$$y = \bar{y}\ (1 - 0.35 \cos \omega t)\ . \tag{12}$$

Reference to Fig. 6 (a trajectory obtained with a digital computer) reveals that this is an excellent approximation.

The interaction of the ion with the ac field is evaluated by assuming that the ion moves as given by Eq. (11) in the nonuniform electric field. The impulse which the ion receives during one radio-frequency cycle is found by integrating the force [Eq. (5)] the ion experiences during the cycle. The acceleration is found through multiplication by the frequency, and division by the mass.

$$\frac{d(mv)}{\text{cycle}} = \int_{\omega t = 0}^{\omega t = 2\pi} F\ dt$$

$$= (1/2)q\ M\ \bar{y}\ \omega \int_{\omega t = 0}^{\omega t = 2\pi} \left[1 - (1/2)q \cos \omega t\right] \cos \omega t\ d\omega t$$

$$= -(1/4)q^2\ M\omega\ \bar{y}\ \pi \tag{13}$$

The acceleration is:

$$\ddot{\bar{y}}_{ac} = -(1/8)\omega^2 q^2 \bar{y} \tag{14}$$

for any value of $\bar{y}$.

The net acceleration of the mean displacement of the ion, averaged over several cycles is the sum of Eqs. (9) and (14).

$$\ddot{\bar{y}} = (1/4)\ \left[a - (1/2)q^2\right]\ \omega^2 \bar{y} \tag{15}$$

The boundary between the stable and the unstable regions of the stability diagram is predicted by this equation when $\ddot{\bar{y}}$ is zero. That is,

$$a = (1/2)q^2. \tag{16}$$

This is to be compared with the exact solution,

$$a = (1/2)q^2 \left[1 - (7/64)q^2 + (29/1152)q^4 \ldots\right]. \tag{17}$$

At the apex, $q = 0.706$, and $a = 0.4755\ q^2$.

Thus, the above expressions for the accelerations are in error by less than 5% at the boundary. Applying this correction to Eq. (15),

$$\ddot{\bar{y}} = 0.25\ (a - 0.4755\ q^2)\ \omega^2 \bar{y}. \tag{18}$$

This adjustment brings the approximate solution into agreement with the formal solution at the apex of the stability triangle. When it is realized that the a, q values of interest in mass spectrometry lie within a few percent of their values at the apex, the merit of the solution obtained by the approximate methods becomes apparent.

Equation (18) may be written as:

$$\ddot{\bar{y}} = 0.25\ (\Delta a)\ \omega^2 y \tag{19}$$

where Δa is the vertical distance from the working point to the y-stability limit, and is positive when the working point is above the stability limit. Within the stable portion of the diagram, Δa is negative, and the quantity $0.25\ (\Delta a)\ \omega^2$ bears a very close resemblance to a spring constant for an undamped, resonant system. Equation (19) is applicable to the y-component of the motion of the ions, for all values of a and q.

Along the scan line (Fig. 4) the spring constant is zero by definition at the y-stability limit. As the working point moves to the right along the scan line, the spring constant increases, causing the ions to be more tightly bound to the y-axis. Concurrently, the spring constant for the x-component of motion weakens, becoming zero at the x-stability limit. Somewhere along the scan line, the spring constants for the x- and for the y-components of motion become equal. Under these conditions the amplitudes for ions which cross the axis with the same x- and y-components of velocities are equal. Paul[1] has postulated, and the calculated trajectories of Figs. 5 and 6 indicate, that this happens when $\beta_x + \beta_y = 1$. The maximum transmission efficiency occurs at this point on the scan line. Let the point of maximum transmission be denoted as a_1, q_1.

Passage of Ions Through the Fringing Fields

As the ions enter the quadrupole through the fringing fields, the intensity of the field varies from zero to the full value which corresponds to the working point, a_1, q_1. In the conventional quadrupole, where the potentials are applied to one set of rods, ratio of the dc to the ac fields in the fringing field region is the same as it is within the quadrupole. HENCE THE WORKING POINT MOVES ALONG THE SCAN LINE, FROM THE ORIGIN TO THE POINT a_1, q_1 AS THE IONS PASS THROUGH THE FRINGING FIELDS. Under conditions of high resolution, when the point a_1, q_1 lies close to the apex, the y-component of motion is unstable for all but a very small portion of this traversal. Further, the degree of instability is very great.

If it is assumed that the point a_1, q_1 lies near the apex and that the equation of the y-stability is that of the parabola expressed by Eq. (15), the maximum value of Δa in the fringing field is readily calculated. It is found to be

$$\Delta a_{max} = a_o/4 = 0.237/4 = 0.05925 \qquad (20)$$

Comparison of Δa_{max} of Eq. (20) with Δa of Eq. (19) reveals that even at modest resolving power the positive acceleration in the radial direction which the ion receives as it traverses the fringing field is many times greater than the acceleration toward the axis within the filter.

When the filter is being used at high resolving power, it is essential that the transit time of the ions through the filter be equal to many periods of the applied ac voltage. This is achieved by using high frequency of excitation, by making a long filter, or by using a low injection energy for the ions. Since a low injection energy for the ions increases the time spent in traversing the fringing field, it increases the radially directed impulse which the ions receive as they traverse the fringing field. Thus, it is seen that the loss of ions owing to traversal of the fringing field is most acute at high resolution settings.

Phase Angle at Time of Ion Entrance into Fields

As the quadrupole is normally used, ions enter the analyzer at all phases of the applied radio-frequency potential. For some time it has been realized that the trajectory of an ion is dependent upon the phase of the voltage at the time of ion entry. Further, it has been appreciated that the importance of phase angle decreases as the number of radio-frequency periods which the ion spends in the fringing field increases.

The mathematical treatment of the trajectory in the quadrupole field requires the help of a computer. However, if the space dependence of the electric field (quadrupole) is simplified to uniform (parallel plate) field, the influence of phase angle is readily assessed. In the mathematical treatment which follows it is assumed that the field is uniform in space, that the ion is formed in a region of full field (does not pass through a fringing field), and that it is at rest at the time of its formation.

Let the ambient field be given by:

$$E = E_o \cos (\omega t + \theta) \tag{21}$$

The force equation is:

$$m\ddot{y} = E_o e \cos (\omega t + \theta) \tag{22}$$

The first integration yields:

$$\dot{y} = \frac{E_o e}{m\omega} \sin (\omega t + \theta) + C_1 \tag{23}$$

The second integration gives:

$$y = - \frac{E_o e}{m\omega^2} \cos (\omega t + \theta) + C_1 t + C_2 \tag{24}$$

The constants of integration are evaluated by the boundary conditions that $y = \dot{y} = 0$ when $t = 0$. This results in:

$$\dot{y} = \frac{E_o e}{m\omega} \left\{ \sin (\omega t + \theta) - \sin \theta \right\} \tag{25}$$

and

$$y = - \frac{E_o e}{m\omega^2} \left\{ \cos (\omega t + \theta) + \omega t \sin \theta - \cos \theta \right\} \tag{26}$$

The first term in Eq. (25) represents the anticipated oscillatory velocity. The second term is zero only for $\theta = n\pi$. For all other phase angles, a constant drift velocity exists. This results from the momentum impulse which the ion receives during its starting transient. Since the magnitude of this impulse is proportional to the field intensity, E_o, it is suggested that if the ion were to enter the field gradually, this impulse would be reduced appreciably.

In the above mathematical derivation it has been assumed that the fields are uniform in space, and thus different from those of the quadrupole. However, since the phenomenon under investigation occurs within the first whole cycle of radio frequency, the impulse given to the ions, as represented by the second term of Eq. (25), is relatively independent

of the field configuration (quadrupole or linear). Thus, the simplifying assumption of uniform field does not reduce the validity of the conclusions, as the ion would not move an appreciable distance and into fields of differing strength, in the time equal to one period of the applied voltage.

PROPOSED METHOD OF ELIMINATING THE Y-INSTABILITY IN THE FRINGING FIELD

Some time ago we[4] suggested that the y-instability in the fringing field be eliminated by reducing the dc component of the electric field in the fringe region. When this is done, the working point remains under (beneath) the y-stability limit as the ion traverses this region. In Fig. 7 the paths taken by the working point as the ion traverses the fringing field are shown for two cases. When one set of electrodes is used, the working point moves along the scan line, as the ratio of the dc to the ac field is everywhere constant. When an auxiliary set of electrodes is used in the vicinity of the entrance aperture, and they are energized with less or zero dc potential as compared to the rods, the working point can be made to follow a path such as that drawn below the y-stability limit.

By causing the working point to move through the stable portion of the diagram, instead of through the y-unstable portion, the very undesirable impulse to the radial velocity is avoided. This is particularly important when the quadrupole is used at higher resolving powers, as the spring constant of Eq. (18) becomes quite weak under these conditions. When this happens, any addition to the radial component of ionic velocity causes the amplitude of the trajectory to become very large. In practical quadrupoles, this means that the ions strike the rods and are not transmitted. It is anticipated that this phenomenon is largely responsible for the acute attenuation of the transmission of ions at high resolving powers (high ratio of dc/ac potentials), as shown by Brubaker and Tuul.[5] Fig. 7 of that paper is included in this report as Fig. 8. Note how rapidly the transmission falls as the ratio of dc to the ac voltages (a/q) increases. As would be expected, the attenuation is more acute for ions which enter farther from the axis, 1/4" aperture vs 1/16" aperture.

---

4. Brubaker, W. M.: Auxiliary Electrodes for Quadrupole Mass Filters. U. S. Patent 3,129,327, April 14, 1964.

5. Brubaker, W. M.; and Tuul, J.: Performance Studies of a Quadrupole Mass Filter. RSI, vol. 35, Aug. 1964, p. 1007.

COMPUTED TRAJECTORIES

A series of computations have been made of ionic trajectories under the influence of quadrupole electric fields. In the specification of the conditions for the calculations, the values of many parameters had to be chosen. First and most important is the locus of the working point in the a - q diagram. Since our interest is in the operation of the quadrupole at moderate resolving power, this point was chosen to give an anticipated resolving power of about 100. It is probable that this same working point (a_1, q_1 = 0.23462, 0.70482) will be used for all calculations.

The working point was chosen to give comparable envelopes for the trajectories in both the x- and the y-directions. This is achieved by selecting a point on the line $\beta_x + \beta_y = 1$. (See Fig. 4.)

Other variables which must be specified for the computations are: entrance position, entrance angle, phase of the applied ac potential at the time the ion enters the field, and the number of cycles the ion spends in traversing the fringing field.

The entrance position was chosen as unity. In almost all cases the amplitude of the trajectory becomes larger than unity. Thus, the amplitude as observed in the trajectory plots tells how far the ion goes from the instrument axis. The units of this distance are the x- or y-distances at which the ions enter the quadrupole. It follows that the ion which enters the field at a distance greater than the distance to the rod, divided by the maximum amplitude of the trajectory, will strike the rod and be lost. The entrance angle was assumed to be zero. Not only is this near to reality in a well-designed ion source, but little new information would be gained by using different angles, since the ion velocity vector is frequently altered appreciably during the first few cycles, owing to the transient, radially directed momentum impulse which the ions receive as they traverse the fringing field. The phase of the ac potential at the time of the entrance of the ion into the field has been made a parameter in several of the series of runs. Special attention is given to the number of ac periods which occur during the passage of the ions through the fringing fields.

When the above variables have been specified, a normalized trajectory is achieved. That is, it is not a function of the instrument size, the magnitude and frequency of the applied voltage, or of the ionic mass.

The first step toward an understanding of this fact is made through reference to Eq. (19). This equation, for constant values of Δa and ω^2, represents simple harmonic motion. Its solution is of the form:

$$y = A \sin \alpha t \tag{27}$$

where $$\alpha = (- \triangle a)^{1/2} \omega \tag{28}$$

Thus it is seen that the ratio of α/ω is uniquely fixed by the variable $\triangle a$.

For all operating conditions the fixed ratio of α/ω determines the distance between successive crossings of the axis. For the assumed conditions of the computations made thus far, the normalized trajectory is independent of the applied frequency. This follows even though the positive accelerations which urge the ions from the axis as well as the negative accelerations which urge them toward the axis are both frequency-dependent. They cancel each other.

For operating conditions in which the ions enter the filter with a radial component of velocity, the amplitude of the trajectory is frequency-dependent, since the negative accelerations which bring this outwardly-directed motion to a halt are proportional to the square of the frequency. The computed trajectories described in this quarterly report do not take this condition into consideration.

While the data obtained from the computed trajectories are most illuminating, and much is to be learned from them, the high cost of using the computer restricts its use to only the most pressing questions. Accordingly, the assumed conditions of operation were chosen with considerable care, in an endeavor to obtain maximum benefits from the computer program.

Four sets of computer runs have been made, and the results are summarized in Figs. 9, 10, and 11. The detailed trajectories are presented in the Appendix. (Figs. A-1 through A-36)

The first set of runs was made under conditions which simulate the formation of ions within the quadrupole structure, where the fields are of full strength. This choice was made to form a base from which the influence of various manners of applying the fields gradually may be assessed. It accurately describes the situation in which ions are formed within the quadrupole either by a laser beam, or perhaps by an electron beam. However, when ions are injected into the quadrupole at high velocity through a geometry which minimizes the effect of the fringing field region, ions may pass through the fringe field in a small fraction of a cycle. This latter condition is quite similar to the assumed one.

To reveal the influence of the phase of the ac potential at the time the ion is formed within the quadrupole, trajectories were computed for

four different phase angles, namely, 0°, 90°, 180°, and 270°. In general, the computations bear out the predictions made by the consideration of linear field conditions. First, the amplitudes are all large for conditions in which large amplitudes are expected (0 = 90°, 270°) and second, in three of the instances in which small amplitudes are predicted (0 = 0°, 180°), they are confirmed. When 0 = 180° the x-component has a large amplitude. This comes about because of the variation of the field with distance from the axis. Under this starting condition the force of the ion is directed outwardly for a quarter cycle. This impulse drives the ion away from the axis, and while the field becomes small and reverses, the ion penetrates deeply into the region of stronger field. (The field is proportional to the distance from the axis.) The maximum amplitudes of the x- and y-trajectories for each of the four starting phase angles are displayed in Fig. 9a.

The assumed conditions for the second and third sets of runs more nearly simulate those of the conventional quadrupole, with one set of four electrodes. Here the ac and the dc fields, in constant proportion, increase linearly with time from zero to full value as the ion traverses the fringing field. These can be described graphically as coincident ramps. For convenience the lengths of the ramps are given in cycles of the applied ac potentials. Ramps of two lengths were considered: two cycles and ten cycles. The two-cycle ramp is as short as would usually be experienced in a practical instrument. The ten-cycle ramp is frequently used when analyzing higher masses. The maximum amplitudes of the trajectories (x and y) resulting from each of four starting phase angles are displayed in Figs. 9b and 9c.

In an earlier section of this report it has been mentioned that the use of an ac ramp, in which the ion enters the strong field region gradually instead of abruptly, may be desirable because the magnitude of the momentum impulse given the ion during its entrance transient is reduced. It is apparent that the two-cycle ramp is effective in reducing the entrance transient and thus in reducing the maximum amplitude, as compared to the conditions in which the ion is introduced into the field abruptly. Because the field is zero at the time the ion enters the fringing region and increases gradually, the influence of the phase at the time of entrance is less than when the ramp is of zero length, as in the first set of runs.

The data for the ten-cycle ramp is quite startling. As expected, the amplitudes of the x-components remain small. The working point for this motion is well removed from the stability limit, and the use of the ramp reduces the entrance transient.

In the y-direction, the operation of the device for a longer time with the working point in the unstable region produces dramatic results. Regardless of the phase angle, the y-amplitude becomes greater than 1000! This fact undoubtedly has considerable bearing upon the data of Fig. 9c, which shows the severe attenuation of the transmission at increasing ratios of dc to ac potentials. As mentioned earlier, this result was anticipated.

Having demonstrated with the computer the great loss of ions by the passage of the y-stability working point through the unstable portion of the diagram, there was great interest in learning of the effectiveness of a previously proposed scheme for eliminating this loss by the use of an additional set (or sets) of electrodes near the entrance aperture. These electrodes are to be energized with lesser portions of dc to ac potentials, relative to the main electrodes (rods). Since the results of the previous runs had shown the small dependence of the amplitudes upon the phase angle when a ramp is used, the phase angle was not changed during this series. Instead, the influence of different manners of applying the dc potentials was investigated. In each case the working point remained below the stability limit. For the fourth set of runs, three normalized patterns with delayed dc ramps were assumed, and for each pattern the length of the ac ramp was made 12 and 24 cycles. The results of these investigations are shown in Fig. 10. Interestingly, in four of the six pairs of trajectories the y-amplitude remained smaller than the x-amplitude.

The prime revelation of these data when compared with previous results (see Fig. 11) is the fact that regardless of the detailed manner in which the dc/ac ratio is tailored, so long as y-stability is maintained by keeping the working point below the stability limit, both maximum x- and y-amplitudes remain quite small. And when it is recalled that the transport of ions is proportional to the square of the effective entrance aperture dimension, the importance of these data is further enhanced.

EXPERIMENTAL APPARATUS

An experimental assembly is being prepared for making tests on the influence of the entrance geometry. A unique feature of this apparatus is the construction of the quadrupole rods. They are ceramic, with evaporated gold surfaces. At the entrance end, each rod has four separate segments, each insulated from the other. The length of each segment is equal to a rod diameter, 0.600 inches. These small segments are followed by two longer sections, 10 inches and 5.5 inches long.

The experimental quadrupole was designed, developed, and fabricated with Corporate funds prior to the initiation of the contract. For these experiments the two longer portions of the rods will be electrically tied together. Through the use of potential dividing networks (both ac and dc) the influence of the potential ramps will be explored.

With this apparatus it is anticipated that the predictions of the computer studies will be experimentally verified. A detailed description of the system will be given in the next report, when experimental data will be presented.

CONCLUSION

The work during the first quarter has been primarily concerned with computer studies of ionic trajectories. This study has verified the predicted vulnerability of conventional quadrupoles to very great loss of ions during operation, especially at high resolving powers. Transmission efficiencies of 0.1% to 1% are indicated by the data. The study also indicates that such losses may be prevented, or at least minimized, through the use of additional sets of quadrupole electrodes.

During the next quarter, laboratory experiments will be conducted on existing Bell & Howell Research Center apparatus to verify the computer-indicated losses and to attempt to eliminate them by the use of additional electrodes. Although experimental conditions will not exactly duplicate those on which the theoretical computations were based, it is anticipated that these experiments will favorably correct present state-of-the-art ion losses.

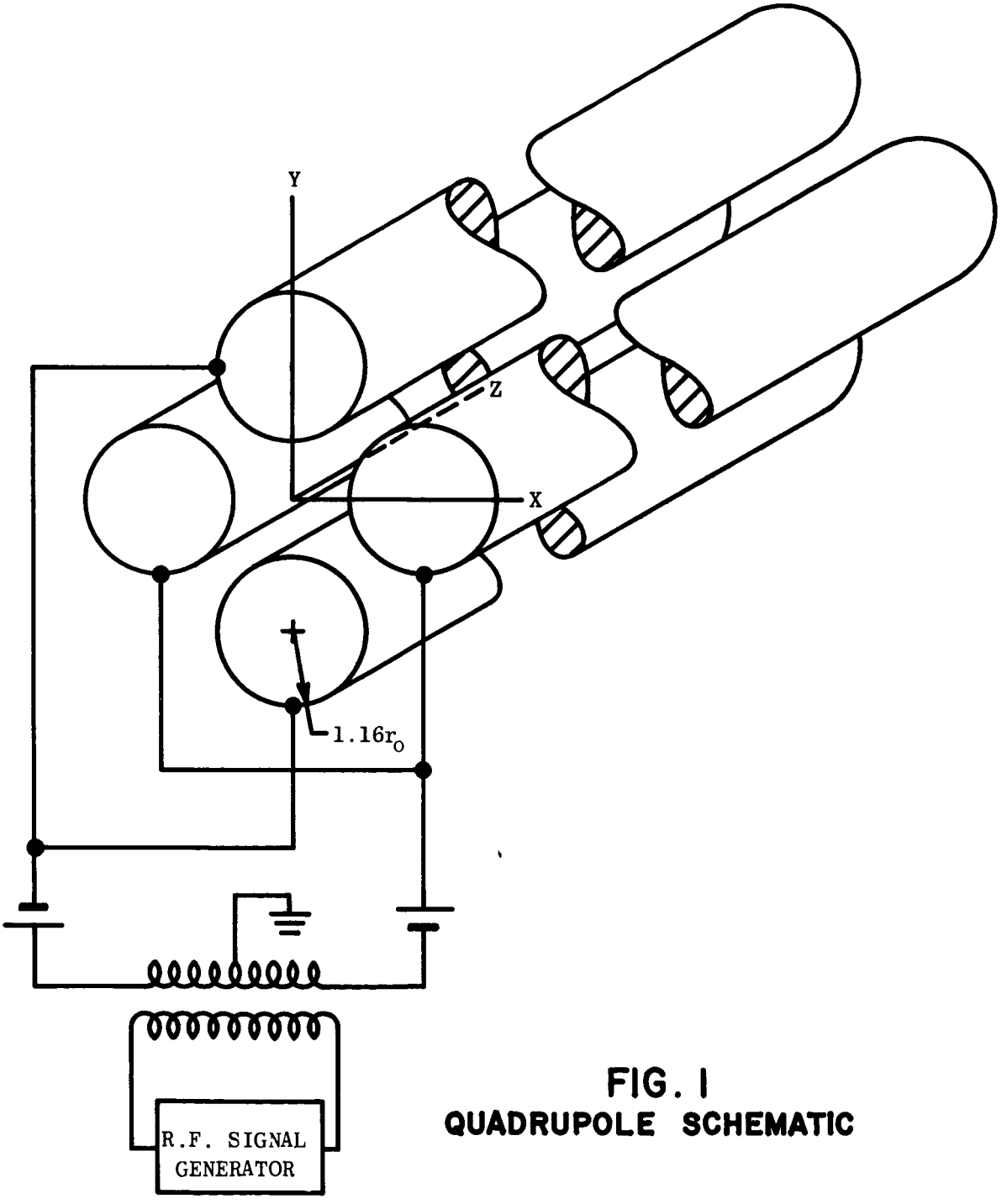

FIG. 1
QUADRUPOLE SCHEMATIC

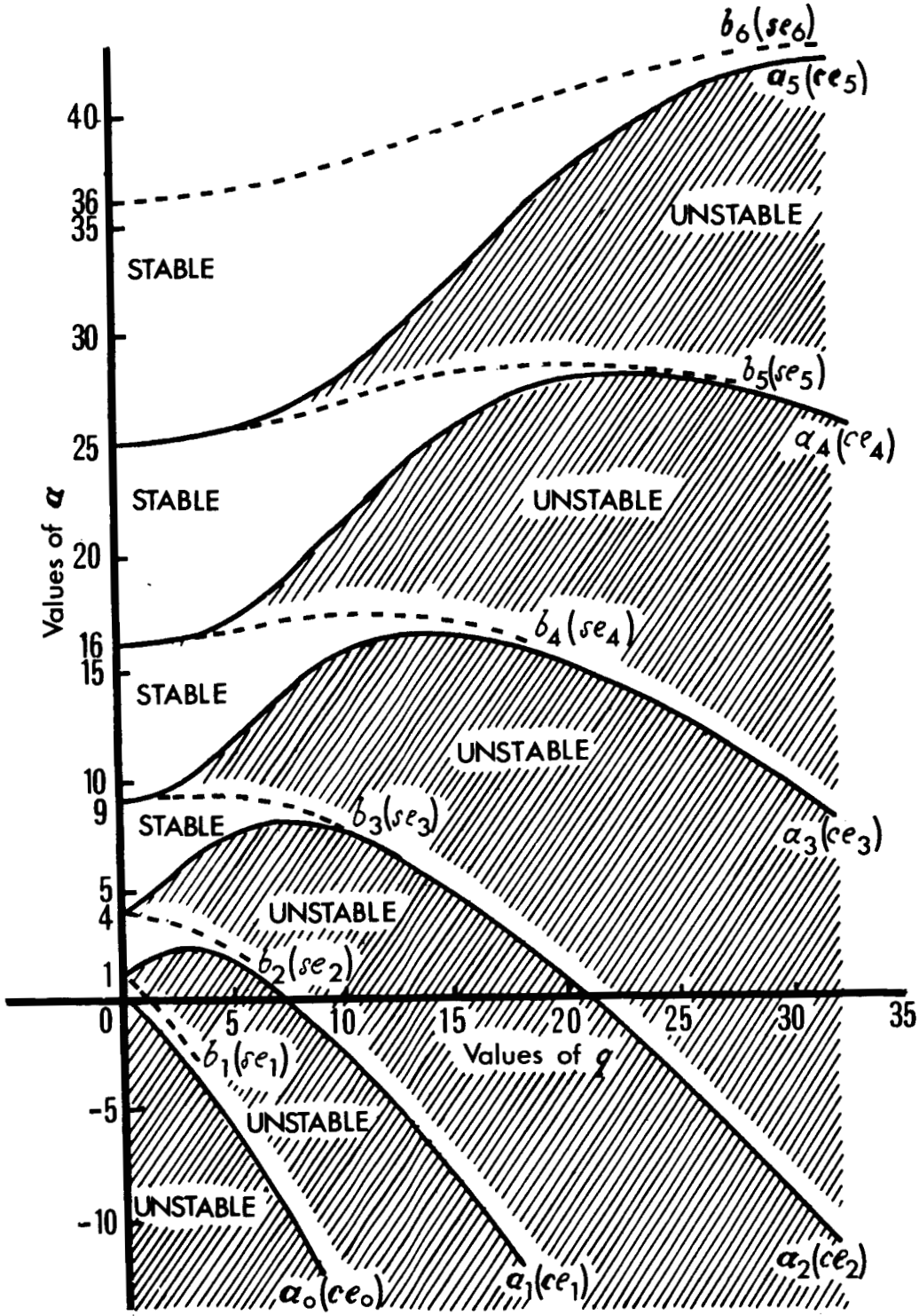

Stability chart for Mathieu functions of integral order. The characteristic curves a_0, b_1, b_2,...divide the plane into regions of stability and instability. The even-order curves are symmetrical, but the odd-order curves are asymmetrical about the a-axis. Nevertheless the diagram is symmetrical about the a-axis.

Fig. 2 - STABILITY CHART

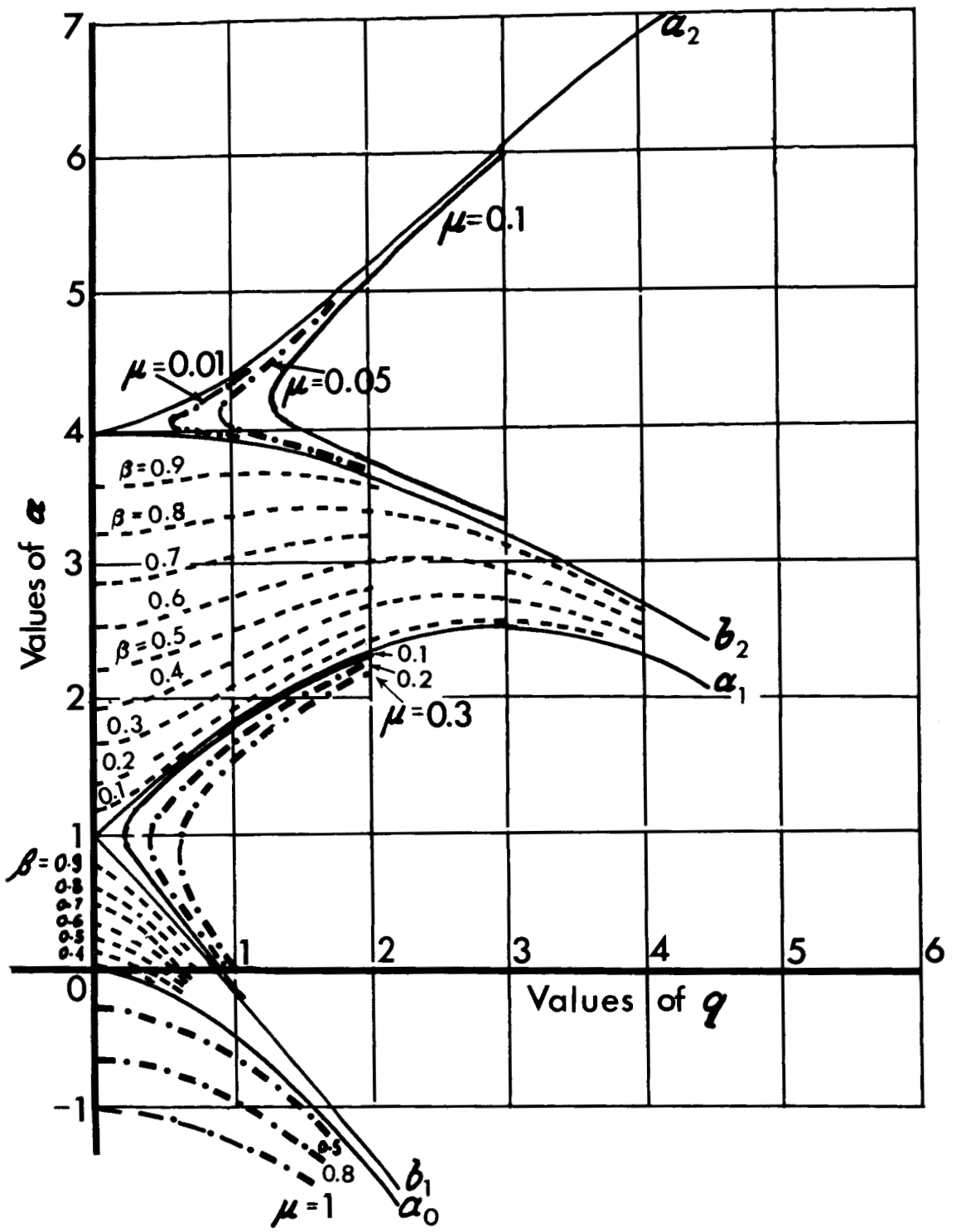

Iso-$\beta\mu$ stability chart for Mathieu functions of fractional order. The iso-β and iso-μ curves are symmetrical about the a-axis.

Fig. 3 - STABILITY CHART

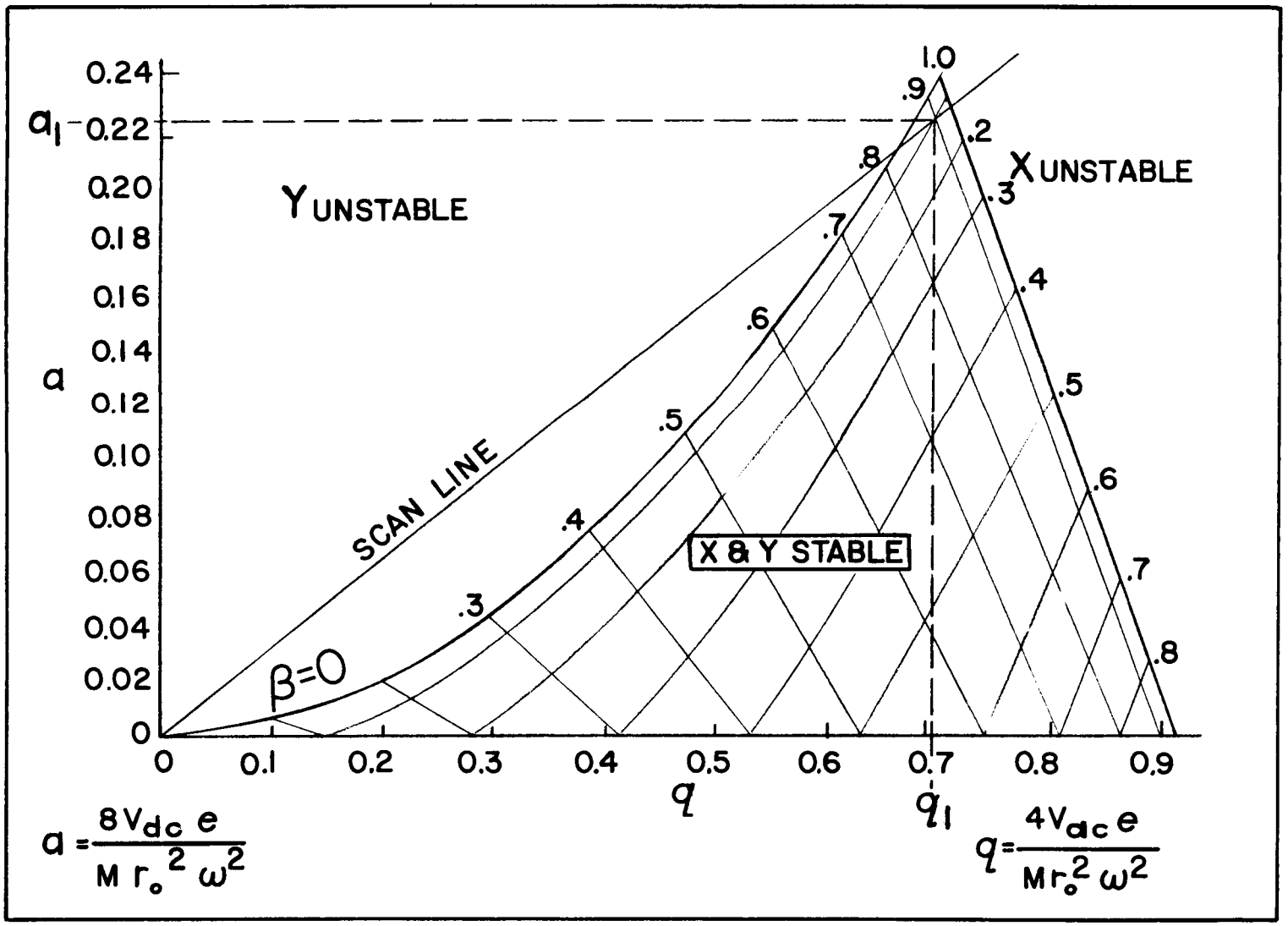

STABILITY DIAGRAM FOR BOTH X & Y

FIGURE 4

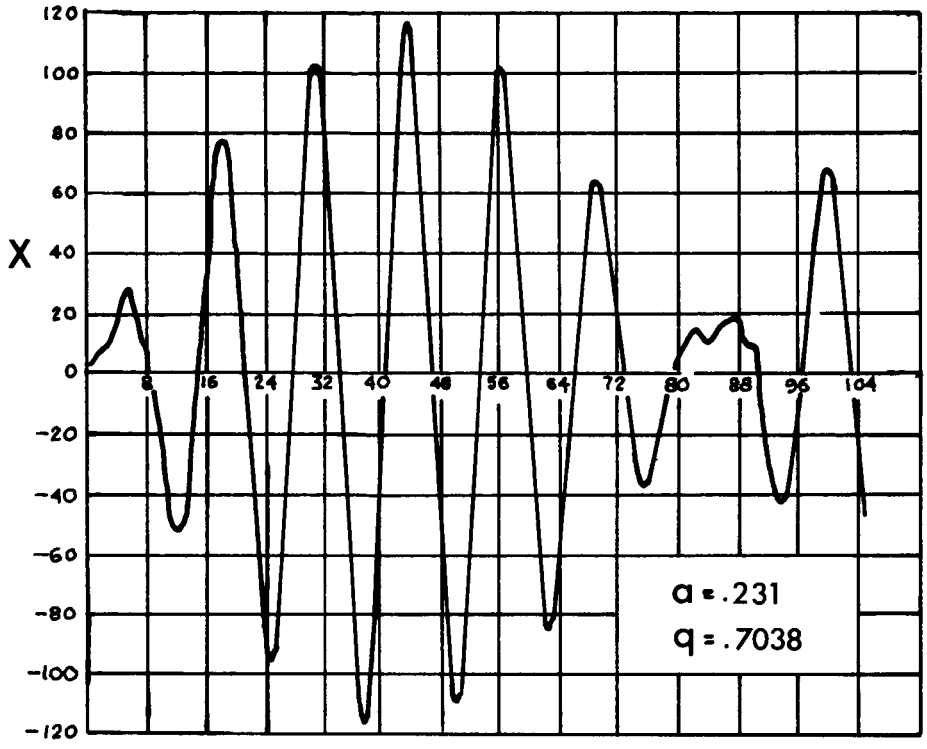

ION TRAJECTORY IN THE X–Z PLANE
FIG. 5

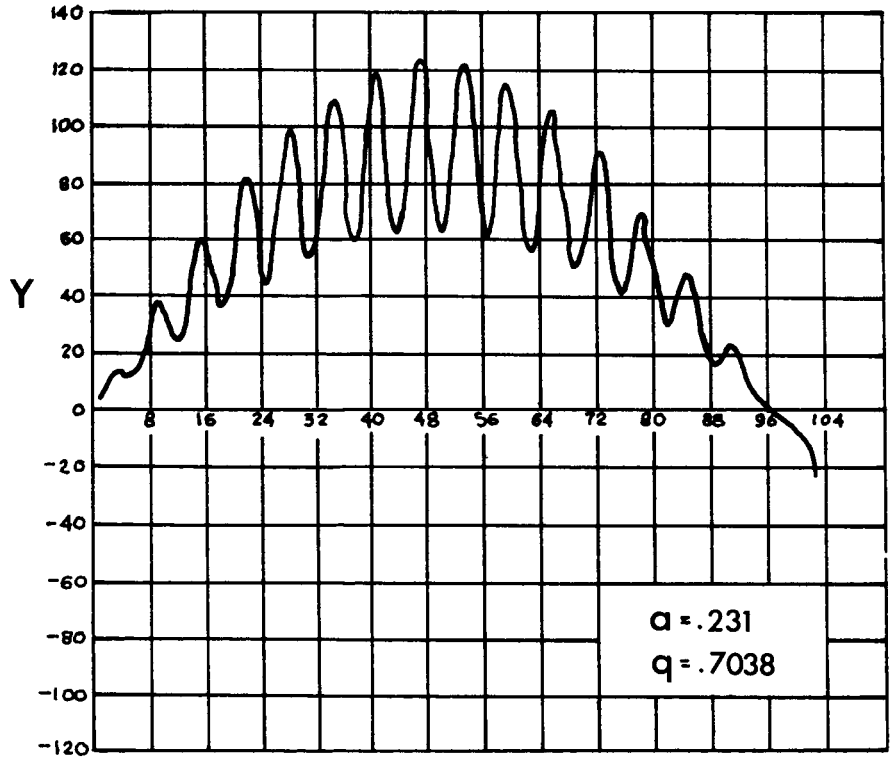

ION TRAJECTORY IN THE Y–Z PLANE
FIG. 6

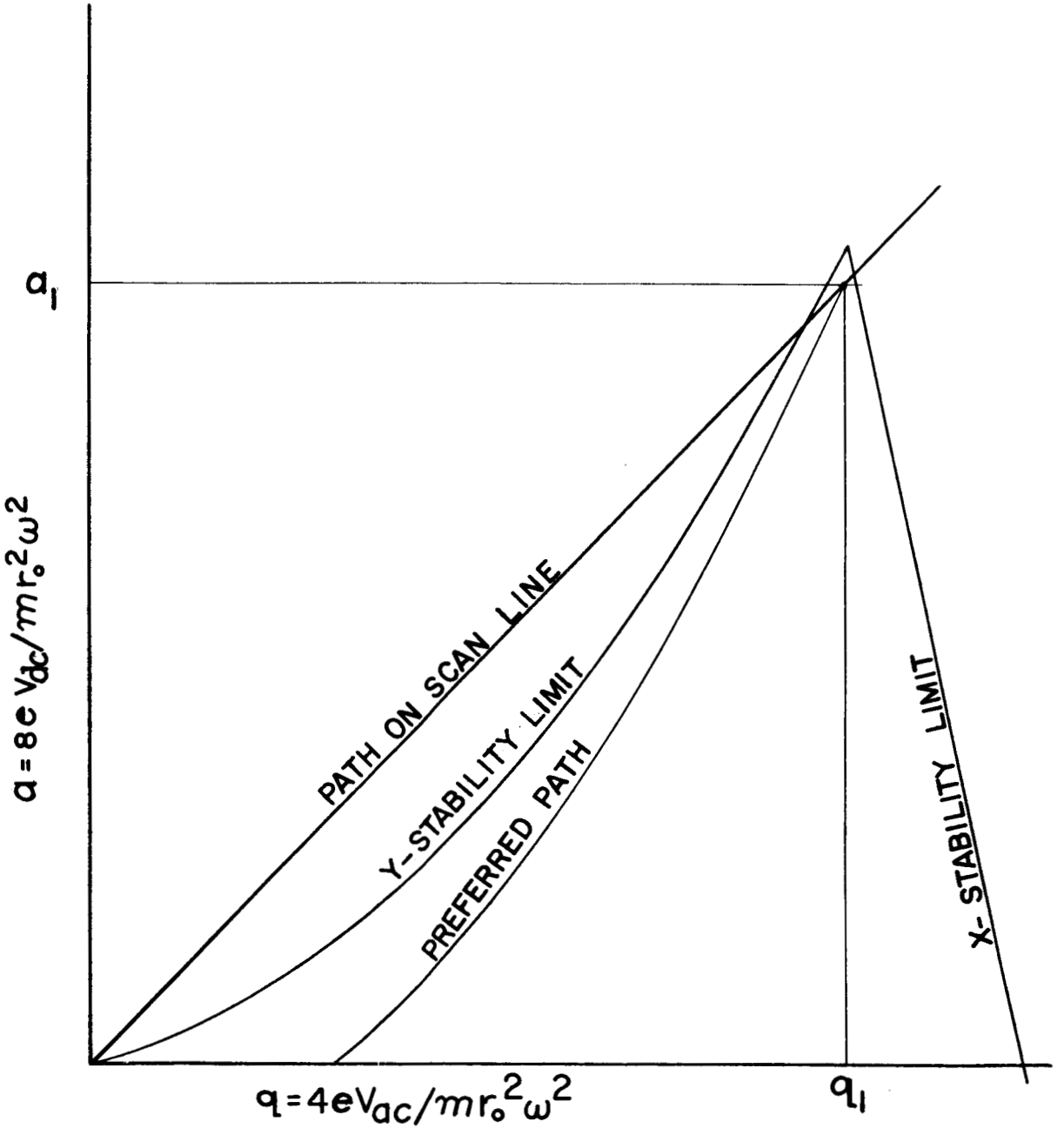

STABILITY DIAGRAM, SHOWING TWO PATHS OF WORKING POINT DURING TRAVERSAL OF FRINGING FIELD.

FIGURE 7

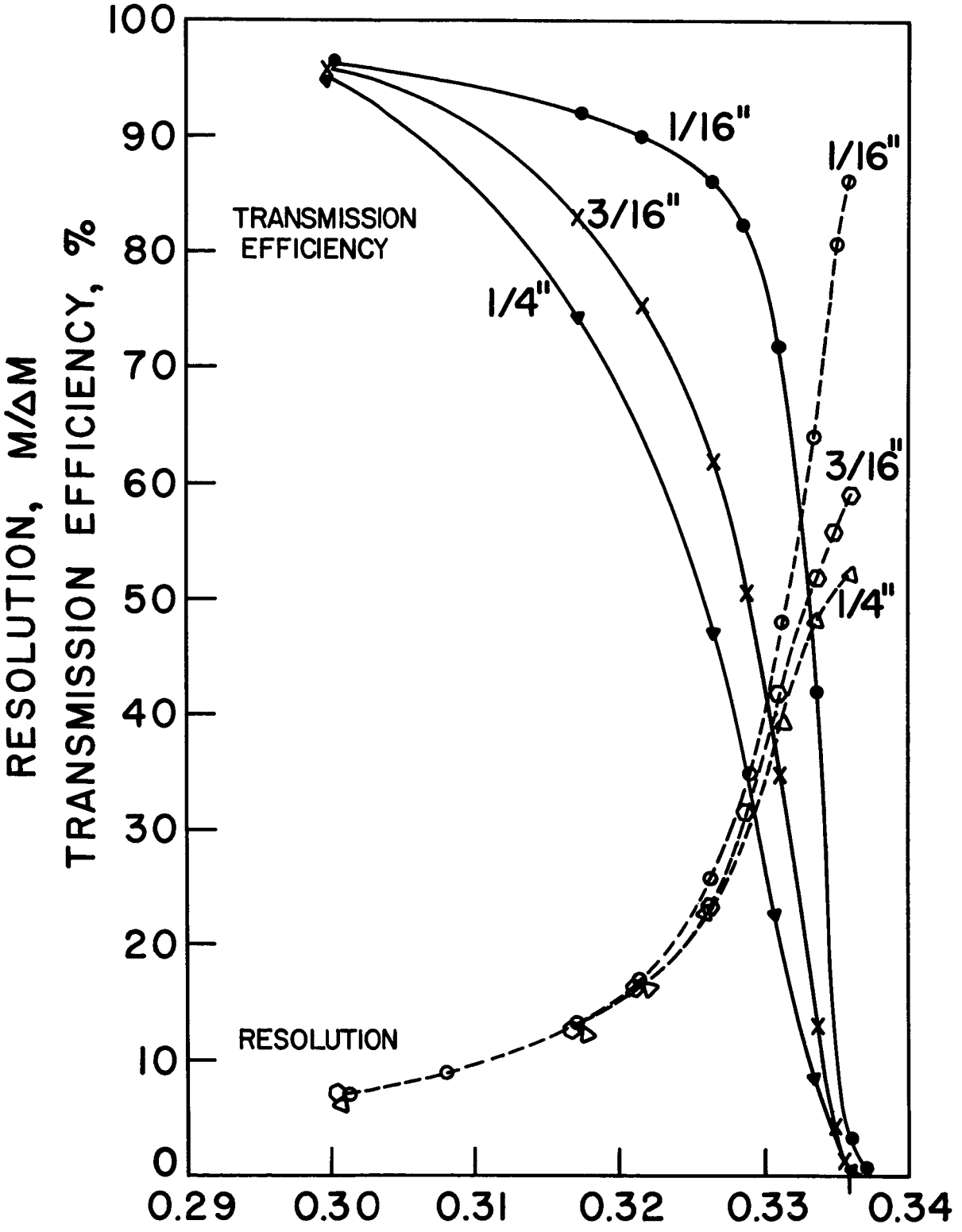
100
90
80
70
60
50
40
30
20
10
0
RESOLUTION, M/ΔM
TRANSMISSION EFFICIENCY, %
TRANSMISSION EFFICIENCY
RESOLUTION
1/16"
3/16"
1/4"
1/16"
3/16"
1/4"
0.29
0.30
0.31
0.32
0.33
0.34
TRANSMISSION EFFICIENCY AND
RESOLUTION AS A FUNCTION OF $\frac{a}{q}$

FIGURE 8

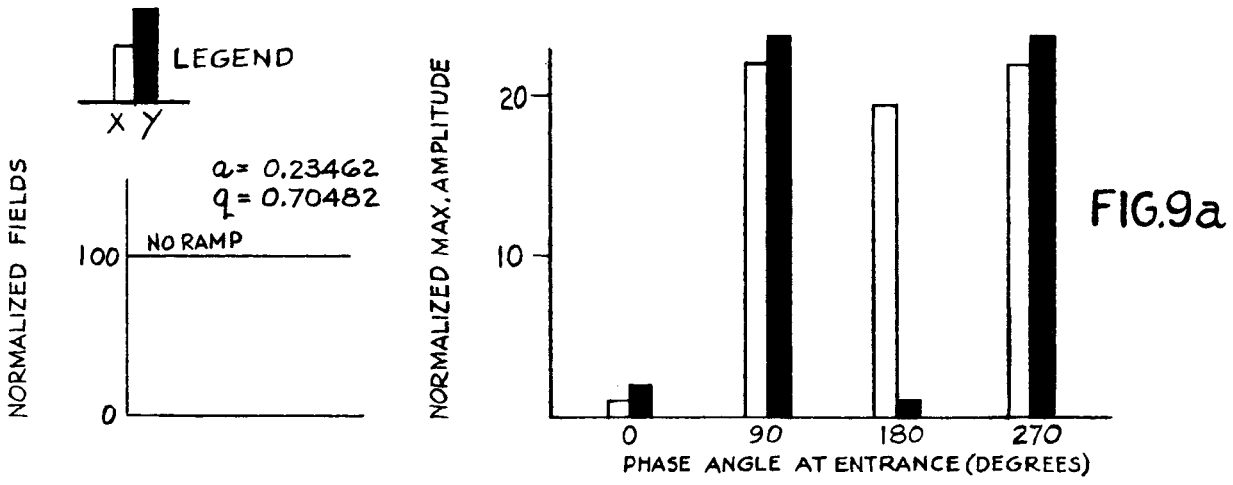

FIG.9a

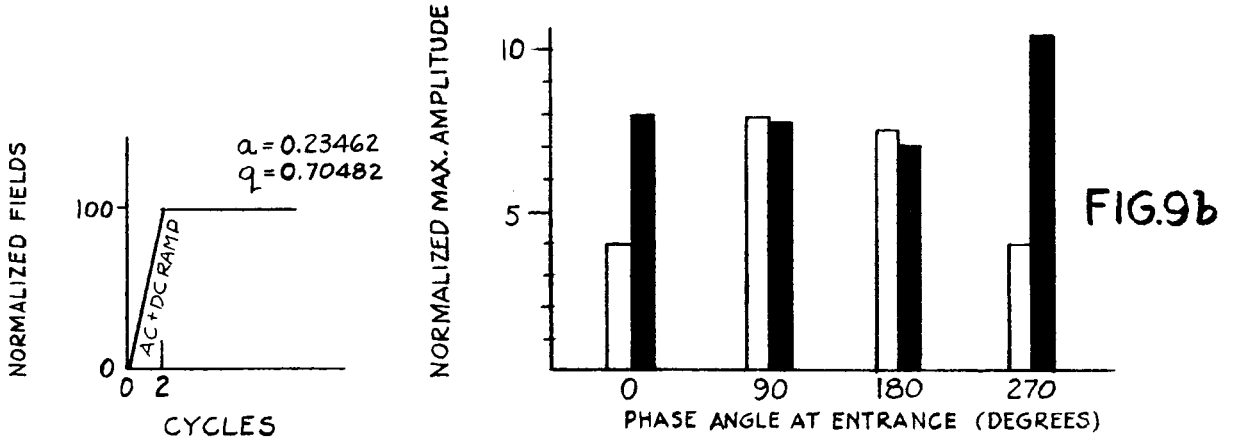

FIG.9b

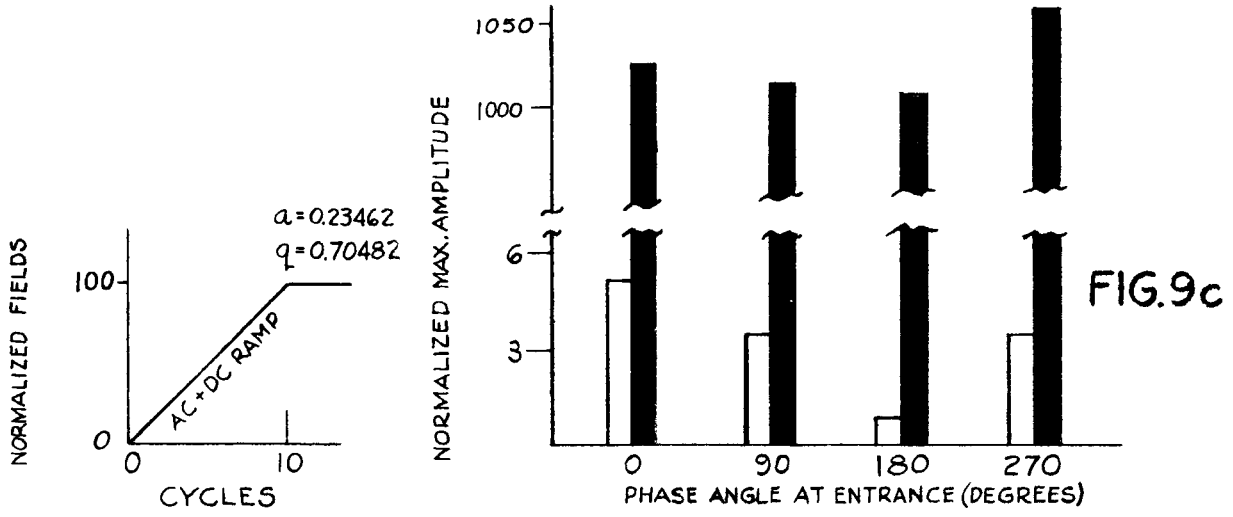

FIG.9c

SUMMARY OF TRAJECTORY PLOTS
WITH COINCIDENT RAMPS

FIG. 9

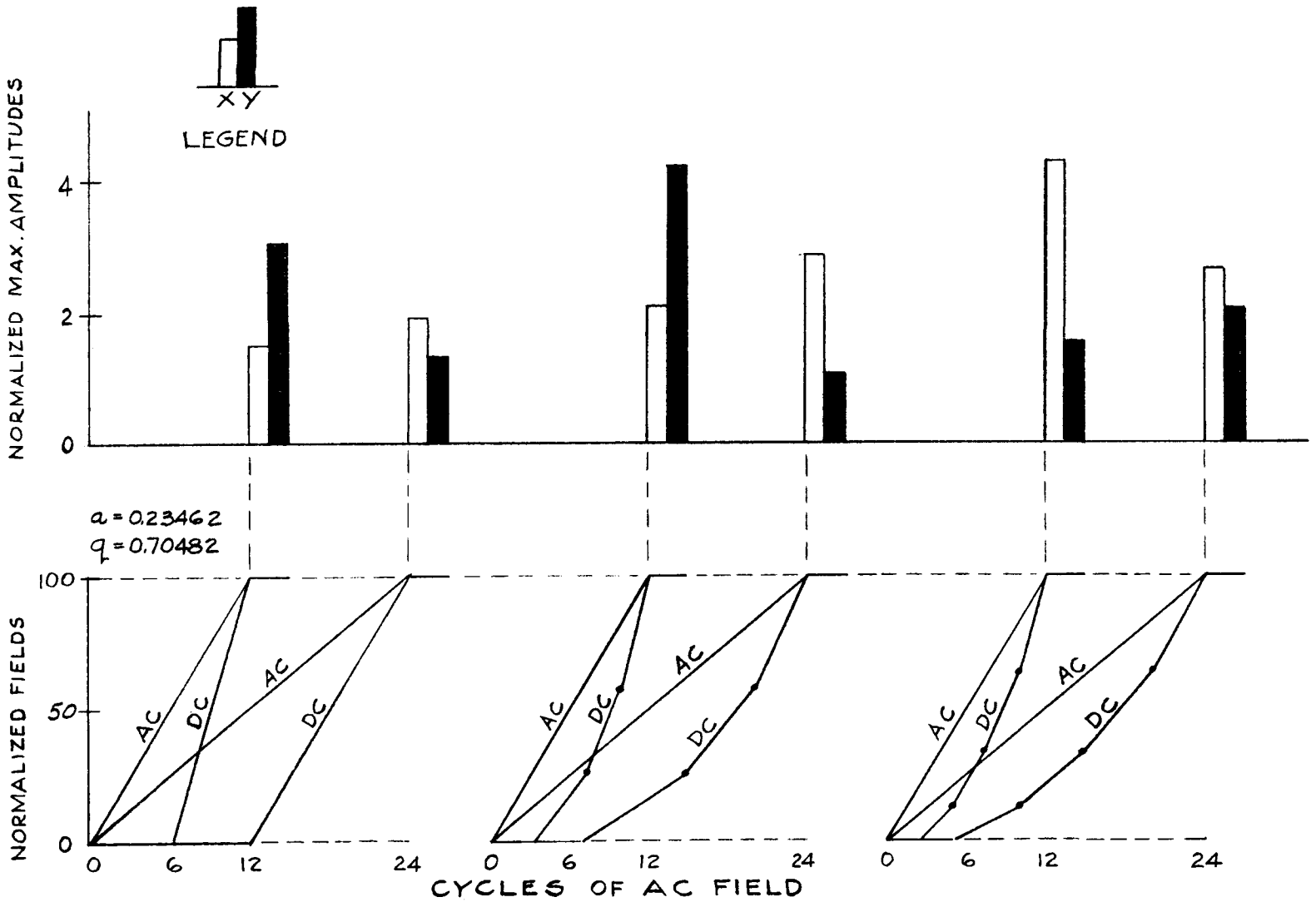

SUMMARY OF TRAJECTORY PLOTS WITH DELAYED D.C. RAMPS

FIG. 10

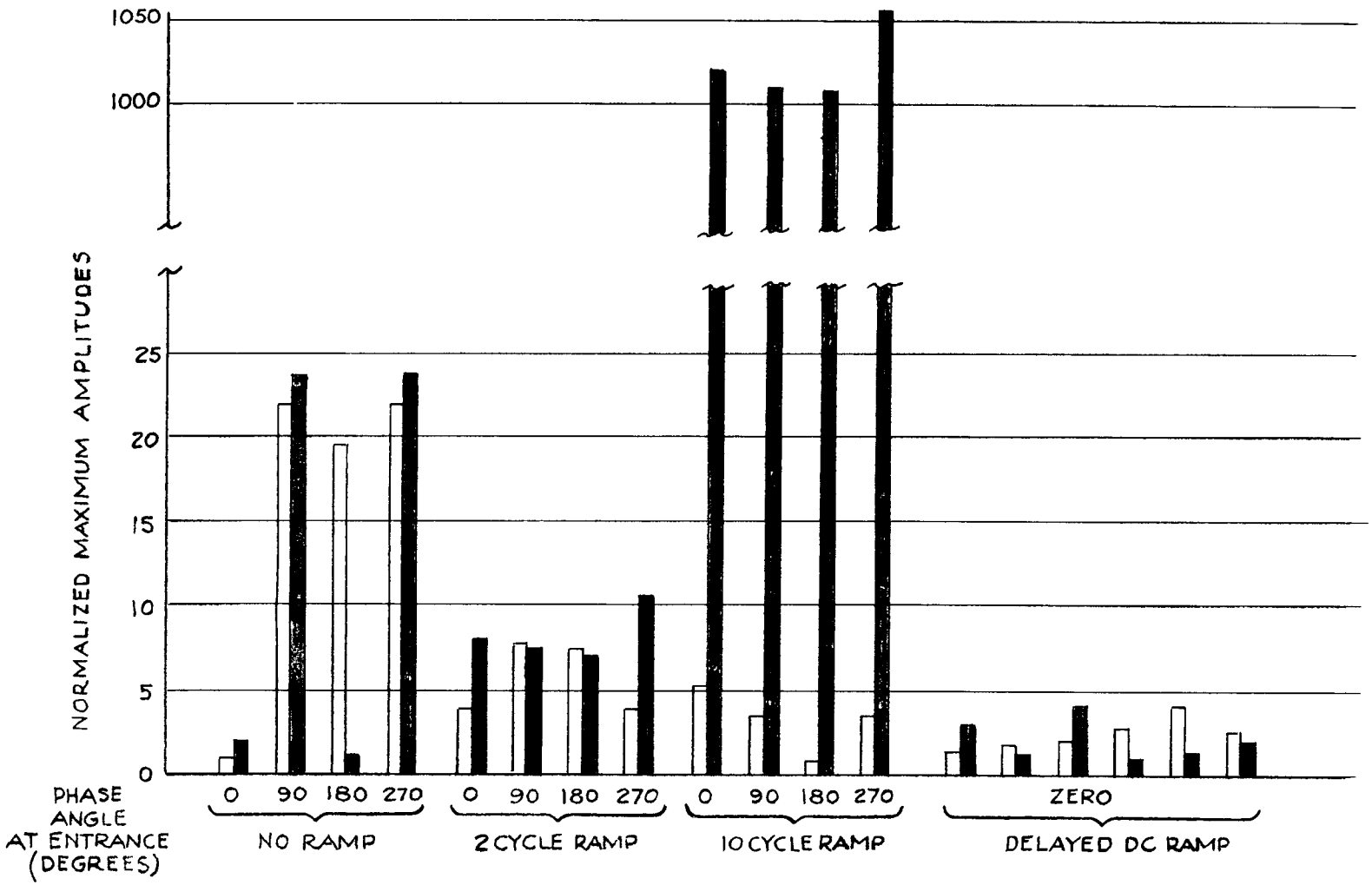

SUMMARY OF ALL TRAJECTORY PLOTS

FIG. 11

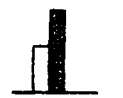

APPENDIX

Introduction

The following 36 pages of the Appendix contain the detailed X and Y trajectory plots (Figs. A-1 through A-36). With the exception of a very few drafting errors, these graphs represent an accurate plot of the data printed out in tabular form from the digital computer. Each point on the graph represents a reversal in the corresponding x- or y-component of velocity. Straight lines were drawn from point to point, and no attempt was made to approximate the actual path of the ion between points. In some cases these lines are quite long because, although still modulated by the ac field, the component of velocity does not reverse.

The variations of the ac and dc fields with respect to time are shown on each of the graphs. On the first eight where the ramp is zero, the representation is a straight line at 100% of normal field strength. In all the other graphs, the exact nature of the coincident and delayed ramps is shown with all changes in slope, marked along the top border in cycles of ac field. Both the field characteristic and the ion trajectory are plotted with respect to ωt.

Table A-1, below, shows the figure numbers in the text in which these detailed plots are summarized.

TABLE A-1

Figures in Appendix	Figure in Text
A-1 through A-8	9a
A-9 through A-16	9b
A-17 through A-24	9c
A-25 through A-36	10
A-1 through A-36	11

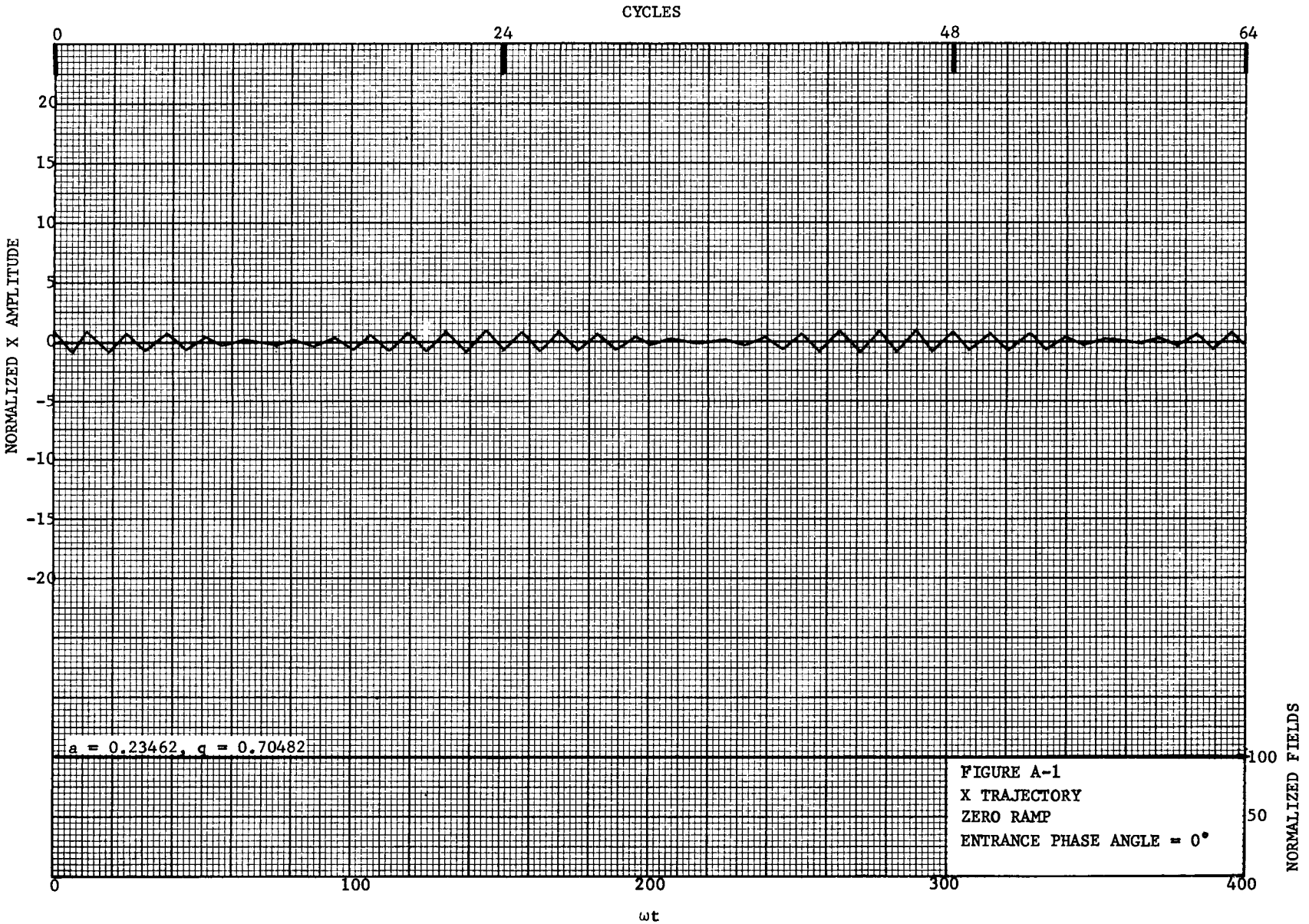

FIGURE A-1
X TRAJECTORY
ZERO RAMP
ENTRANCE PHASE ANGLE = 0°

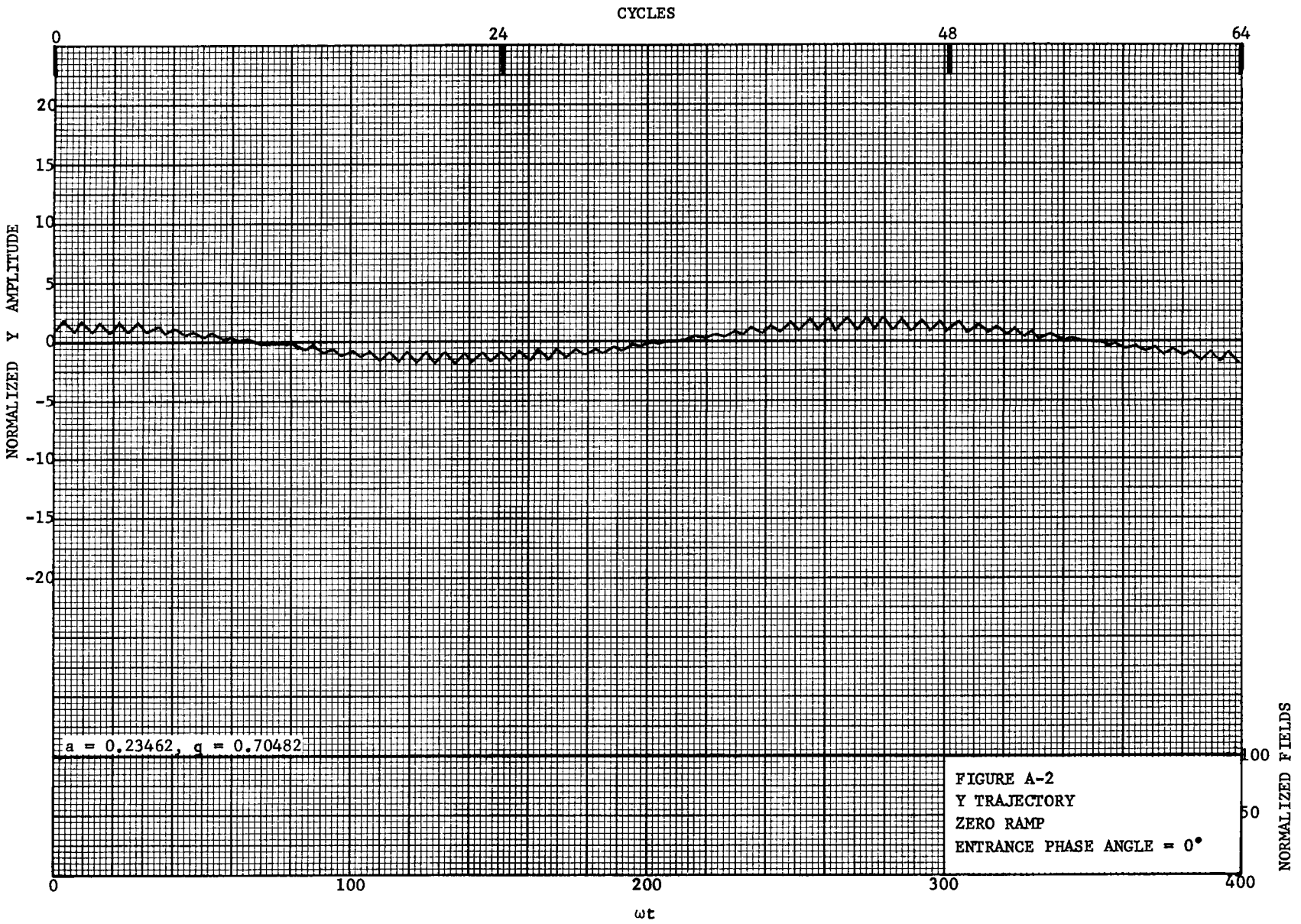

FIGURE A-2
Y TRAJECTORY
ZERO RAMP
ENTRANCE PHASE ANGLE = 0°

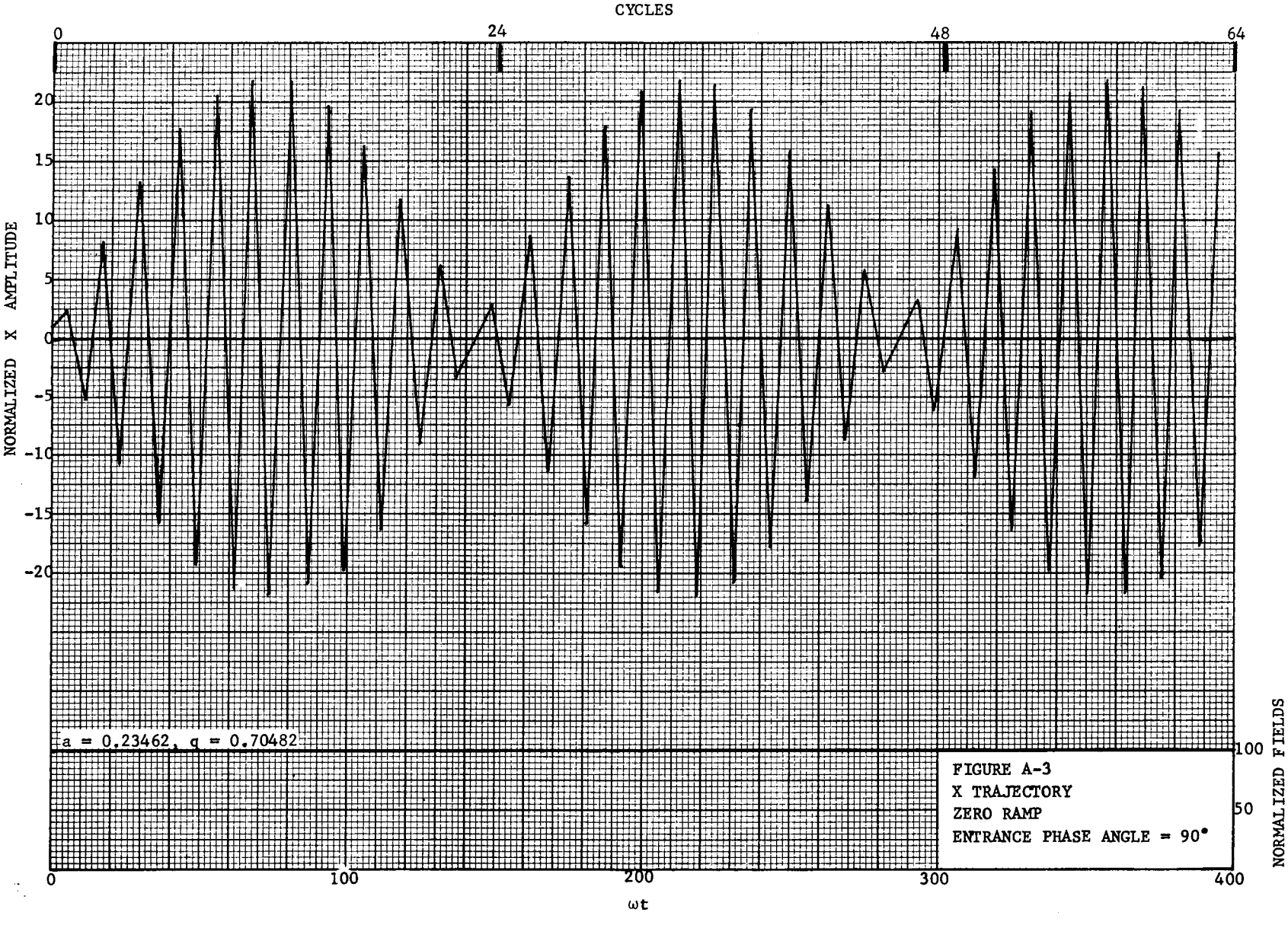

FIGURE A-3
X TRAJECTORY
ZERO RAMP
ENTRANCE PHASE ANGLE = 90°

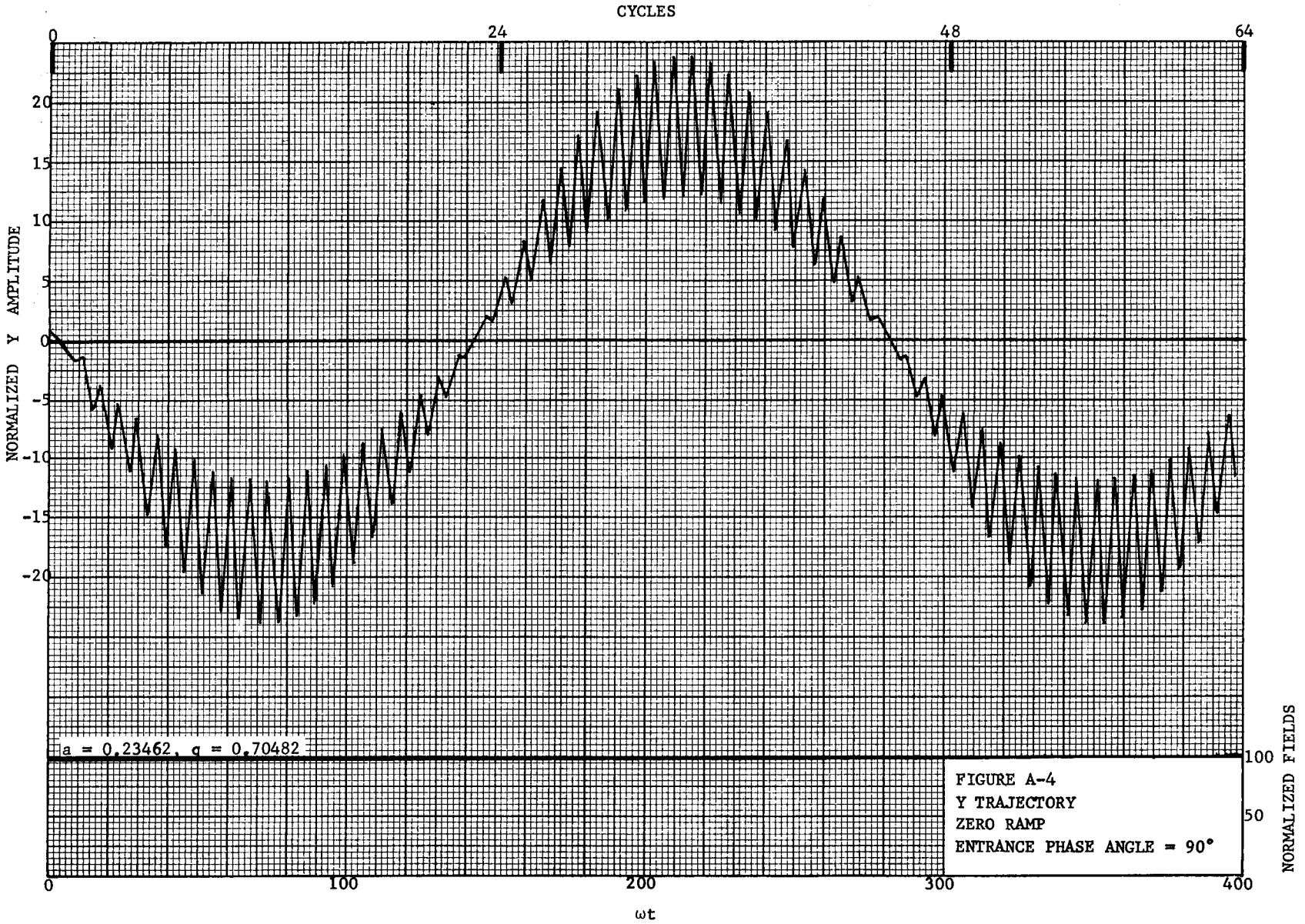

FIGURE A-4
Y TRAJECTORY
ZERO RAMP
ENTRANCE PHASE ANGLE = 90°

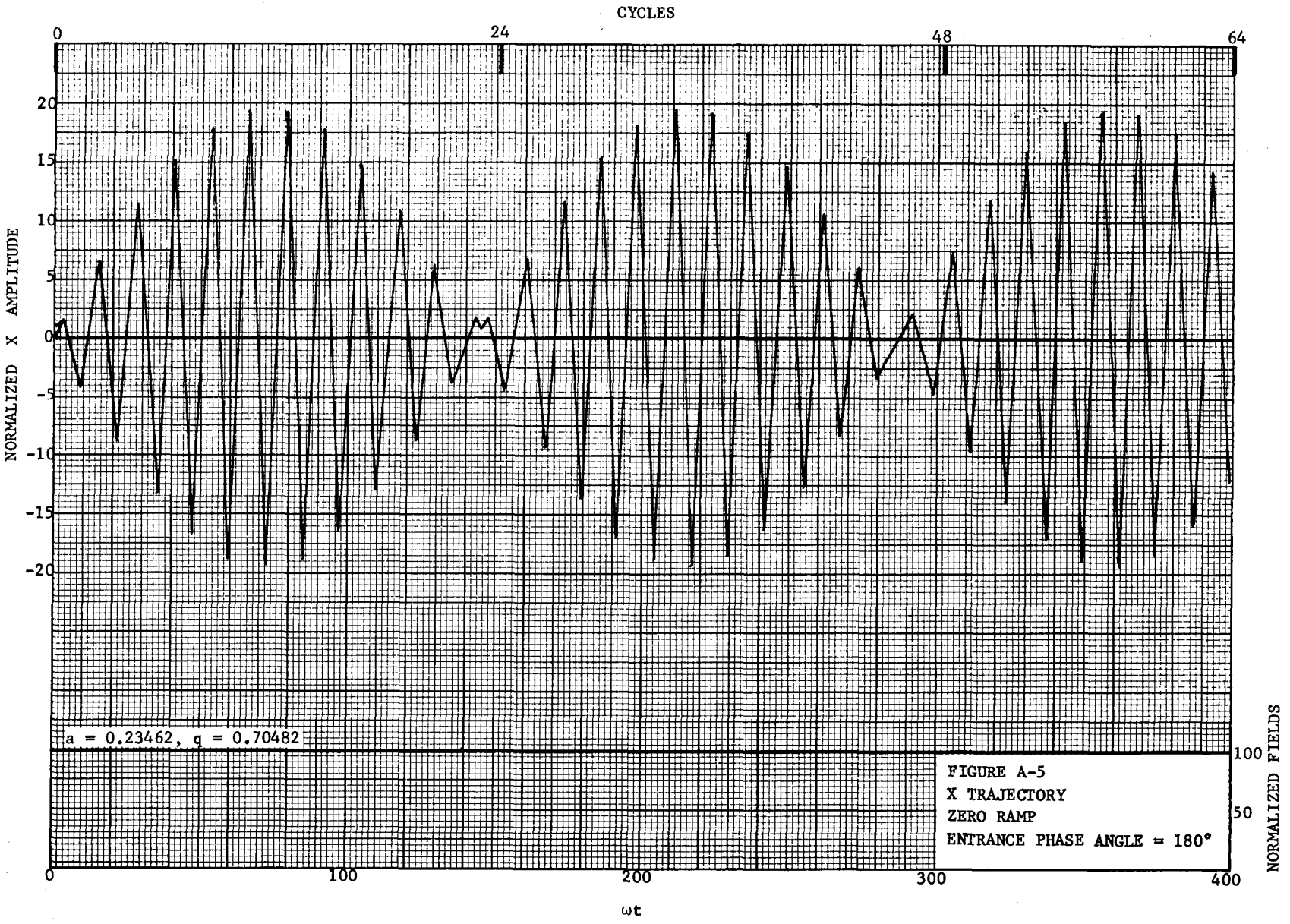

FIGURE A-5
X TRAJECTORY
ZERO RAMP
ENTRANCE PHASE ANGLE = 180°

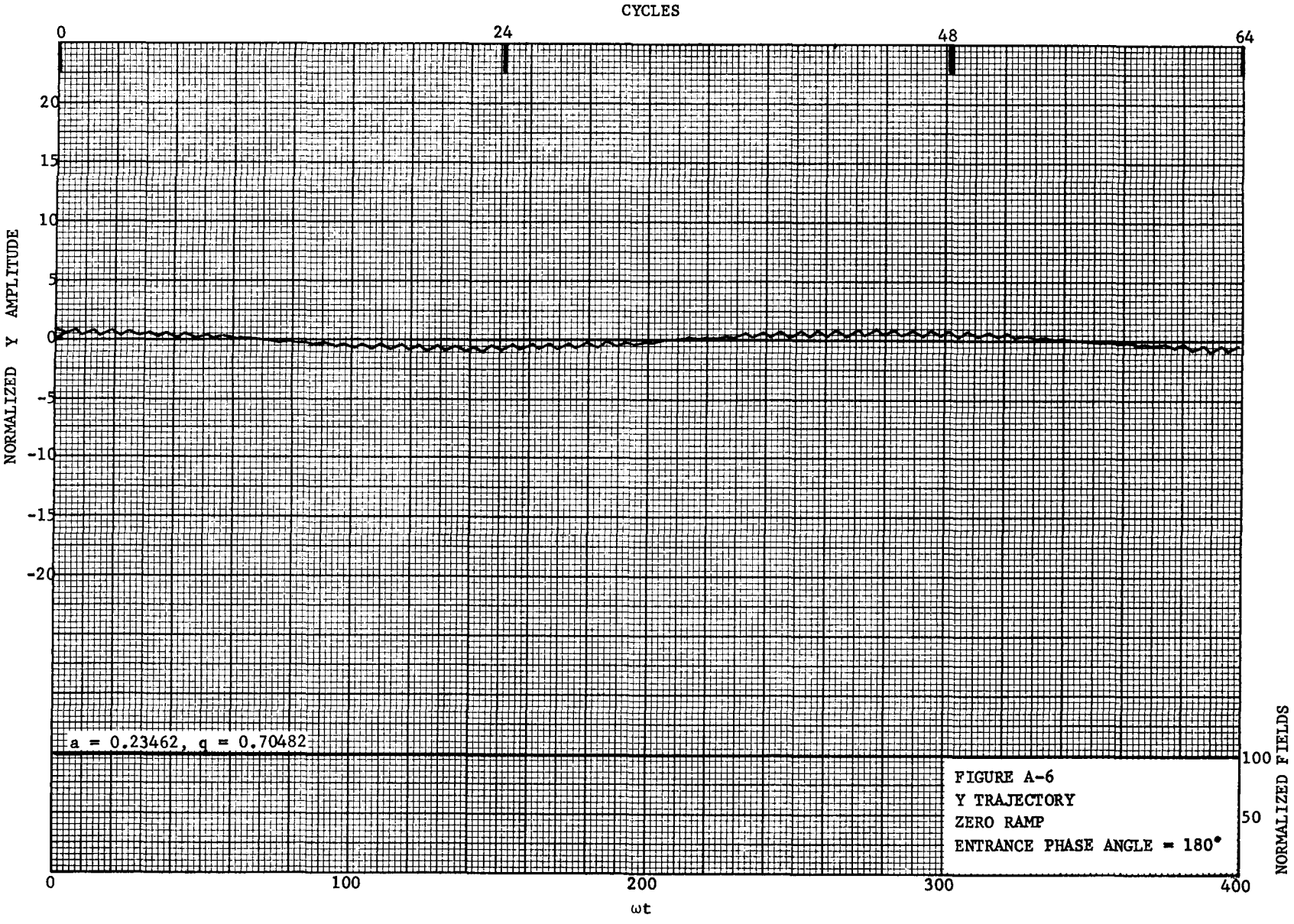

FIGURE A-6
Y TRAJECTORY
ZERO RAMP
ENTRANCE PHASE ANGLE = 180°

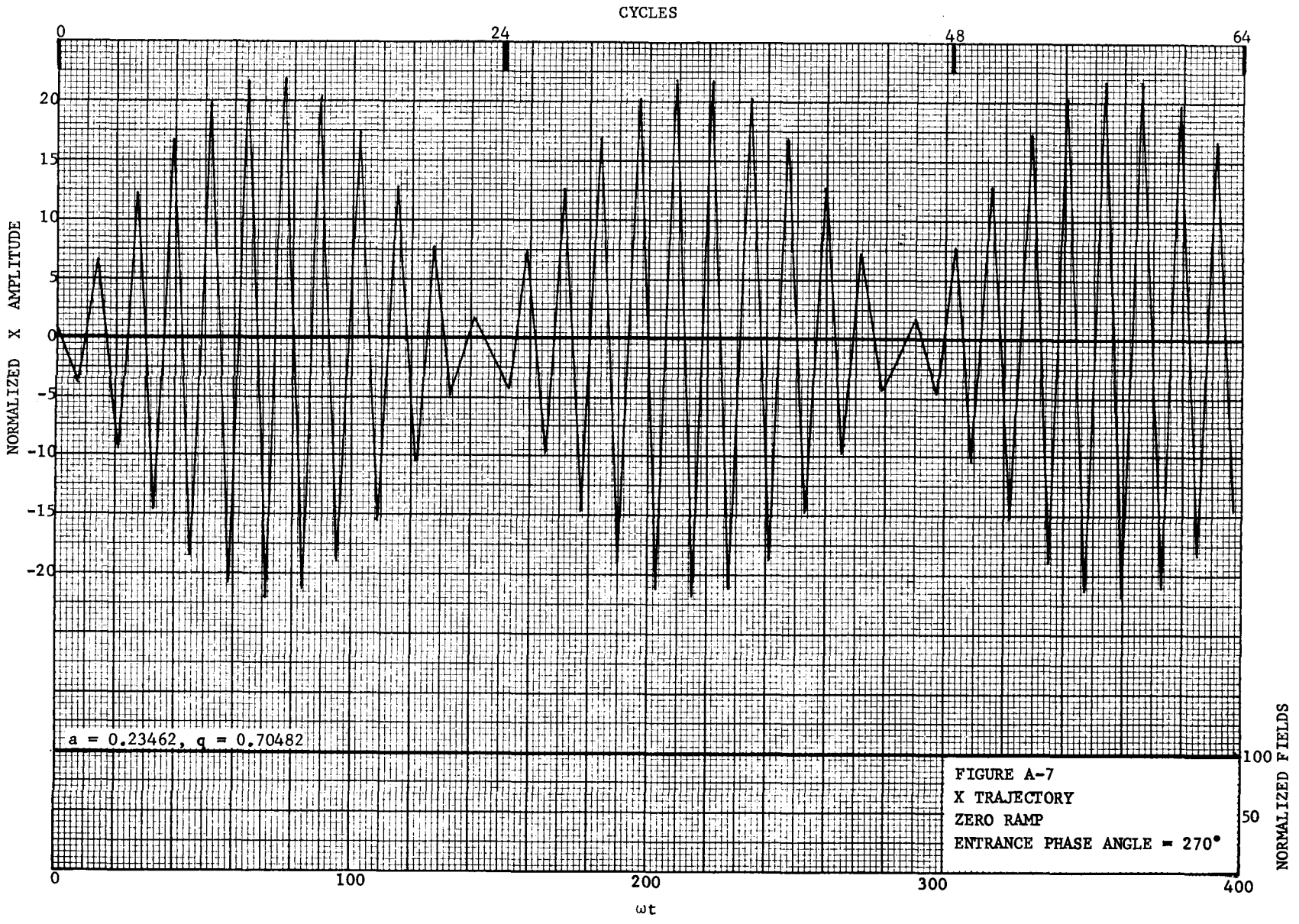

FIGURE A-7
X TRAJECTORY
ZERO RAMP
ENTRANCE PHASE ANGLE = 270°

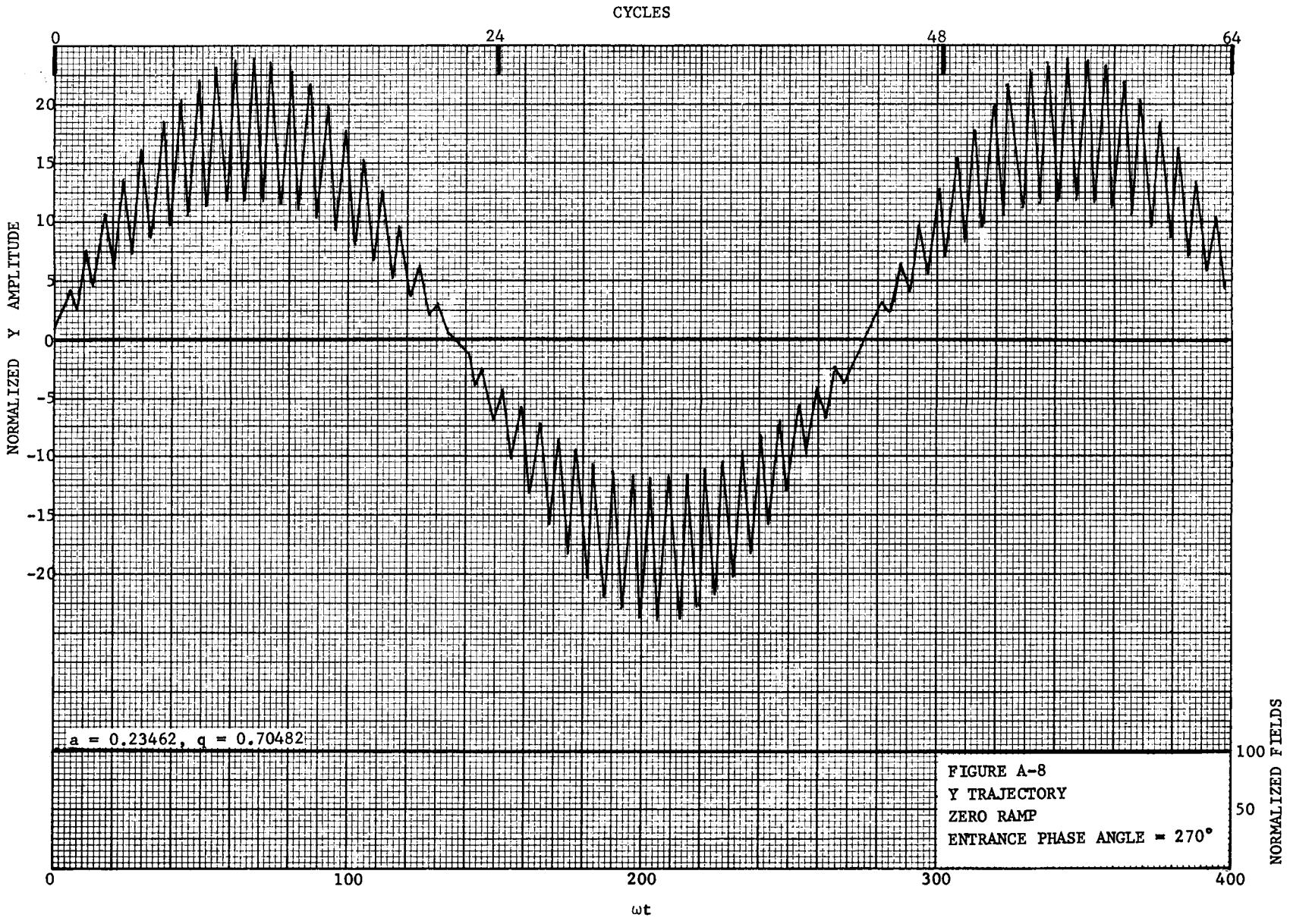

FIGURE A-8
Y TRAJECTORY
ZERO RAMP
ENTRANCE PHASE ANGLE = 270°

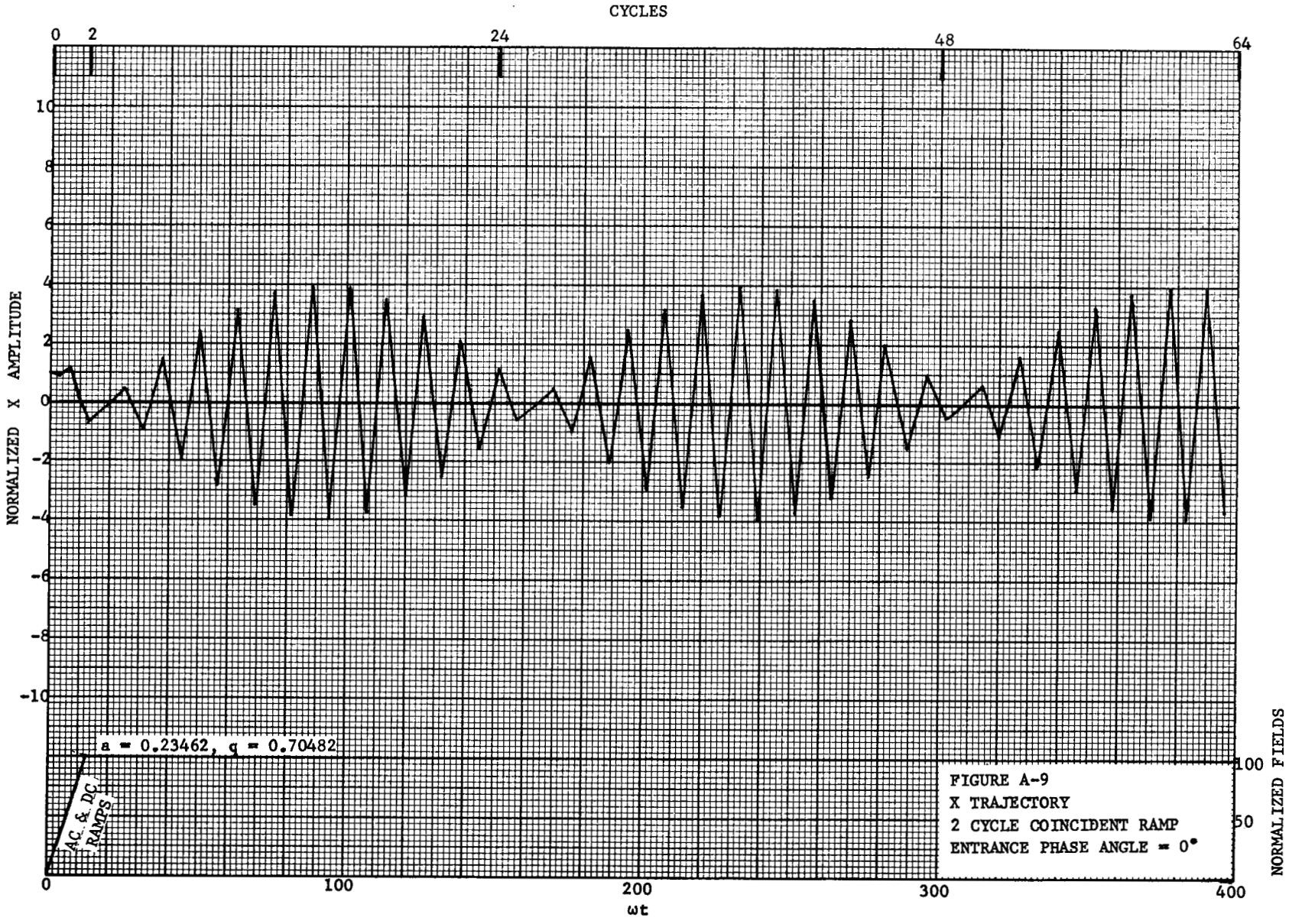
CYCLES
0
2
24
48
64
10
8
6
4
2
0
-2
-4
-6
-8
-10
NORMALIZED X AMPLITUDE
a = 0.23462, q = 0.70482
A.C. & D.C. RAMPS
0
100
200
300
400
ωt
100
50
NORMALIZED FIELDS
FIGURE A-9
X TRAJECTORY
2 CYCLE COINCIDENT RAMP
ENTRANCE PHASE ANGLE = 0°

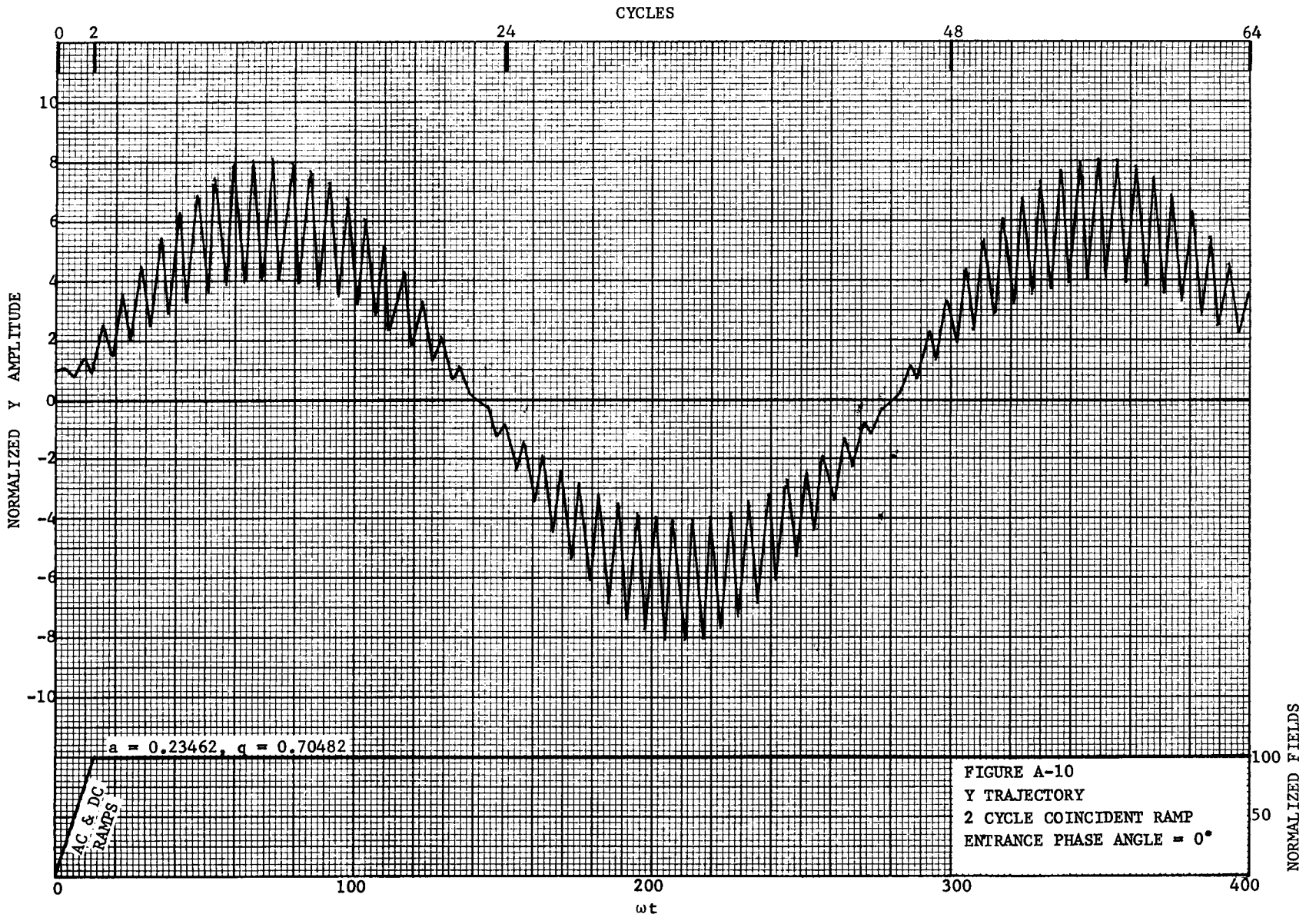

FIGURE A-10
Y TRAJECTORY
2 CYCLE COINCIDENT RAMP
ENTRANCE PHASE ANGLE = 0°

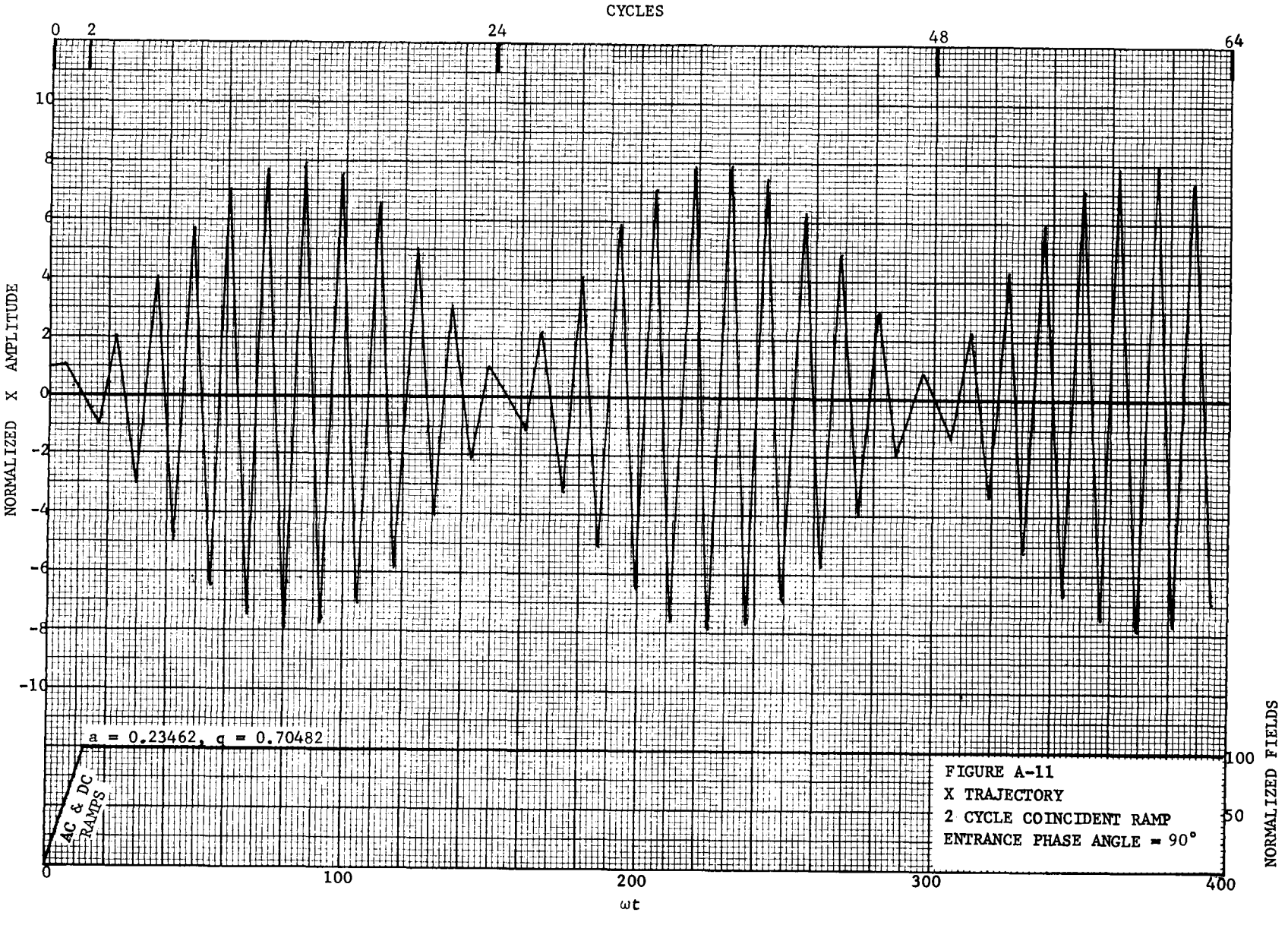

FIGURE A-11
X TRAJECTORY
2 CYCLE COINCIDENT RAMP
ENTRANCE PHASE ANGLE = 90°

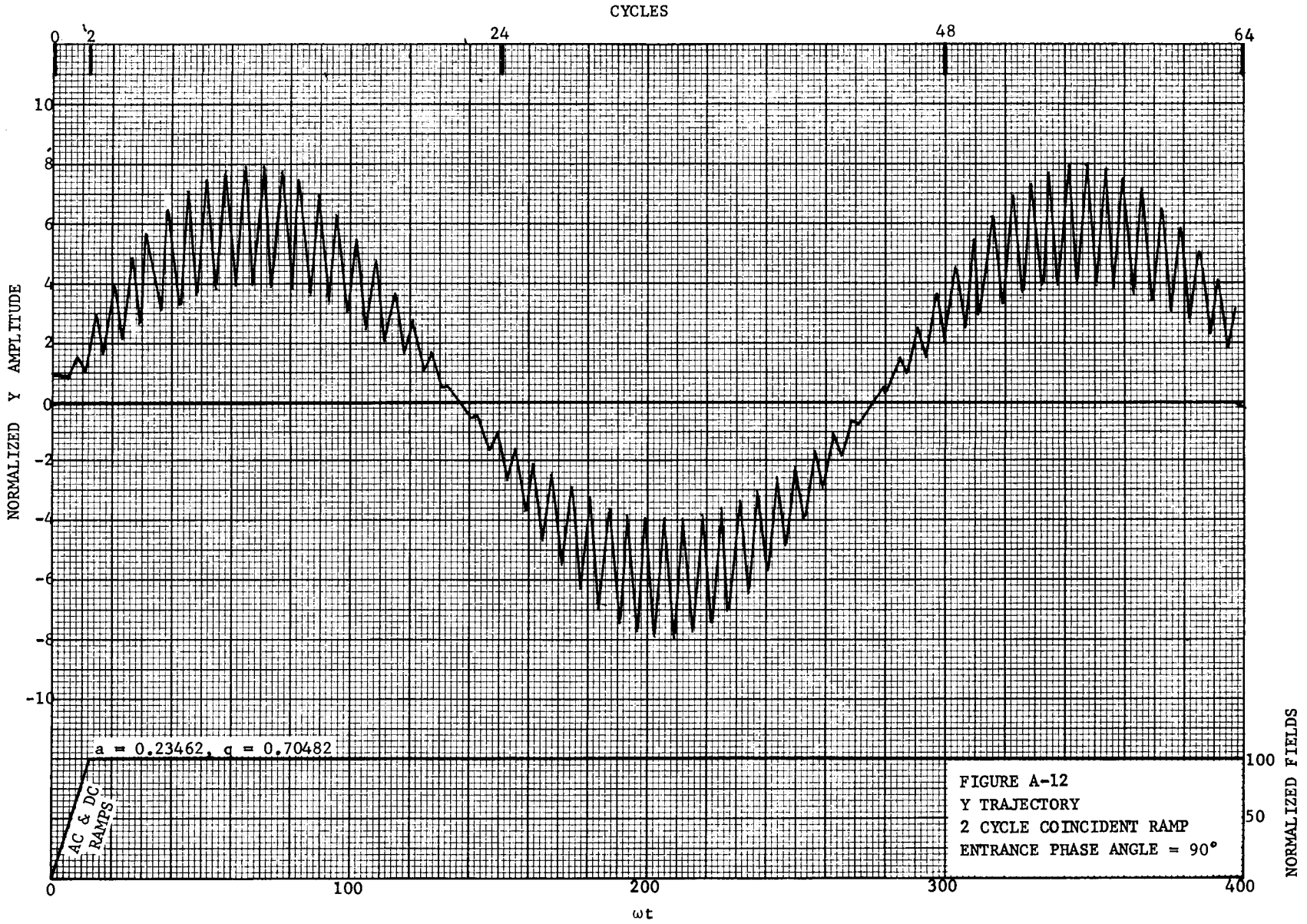

FIGURE A-12
Y TRAJECTORY
2 CYCLE COINCIDENT RAMP
ENTRANCE PHASE ANGLE = 90°

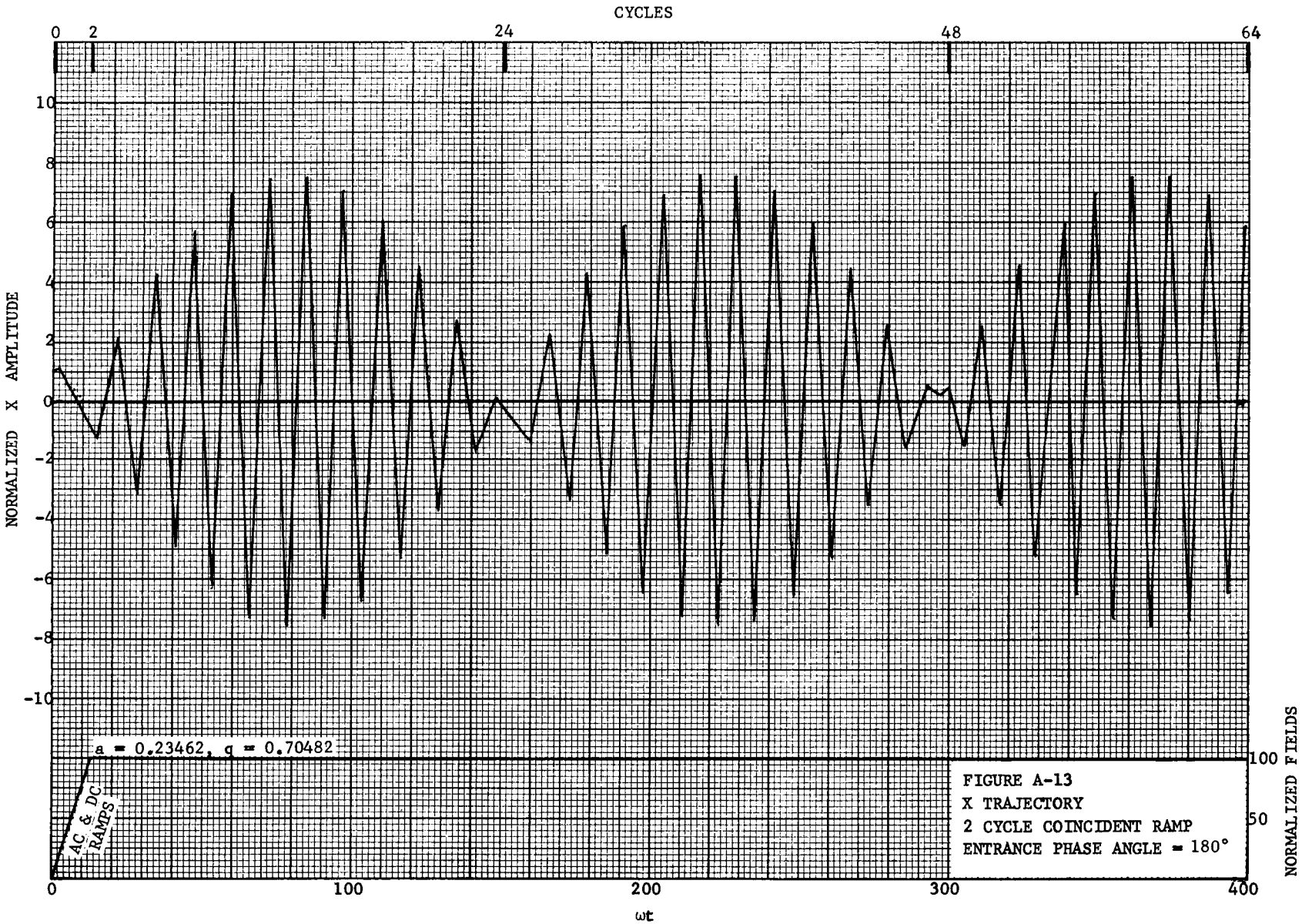

FIGURE A-13
X TRAJECTORY
2 CYCLE COINCIDENT RAMP
ENTRANCE PHASE ANGLE = 180°

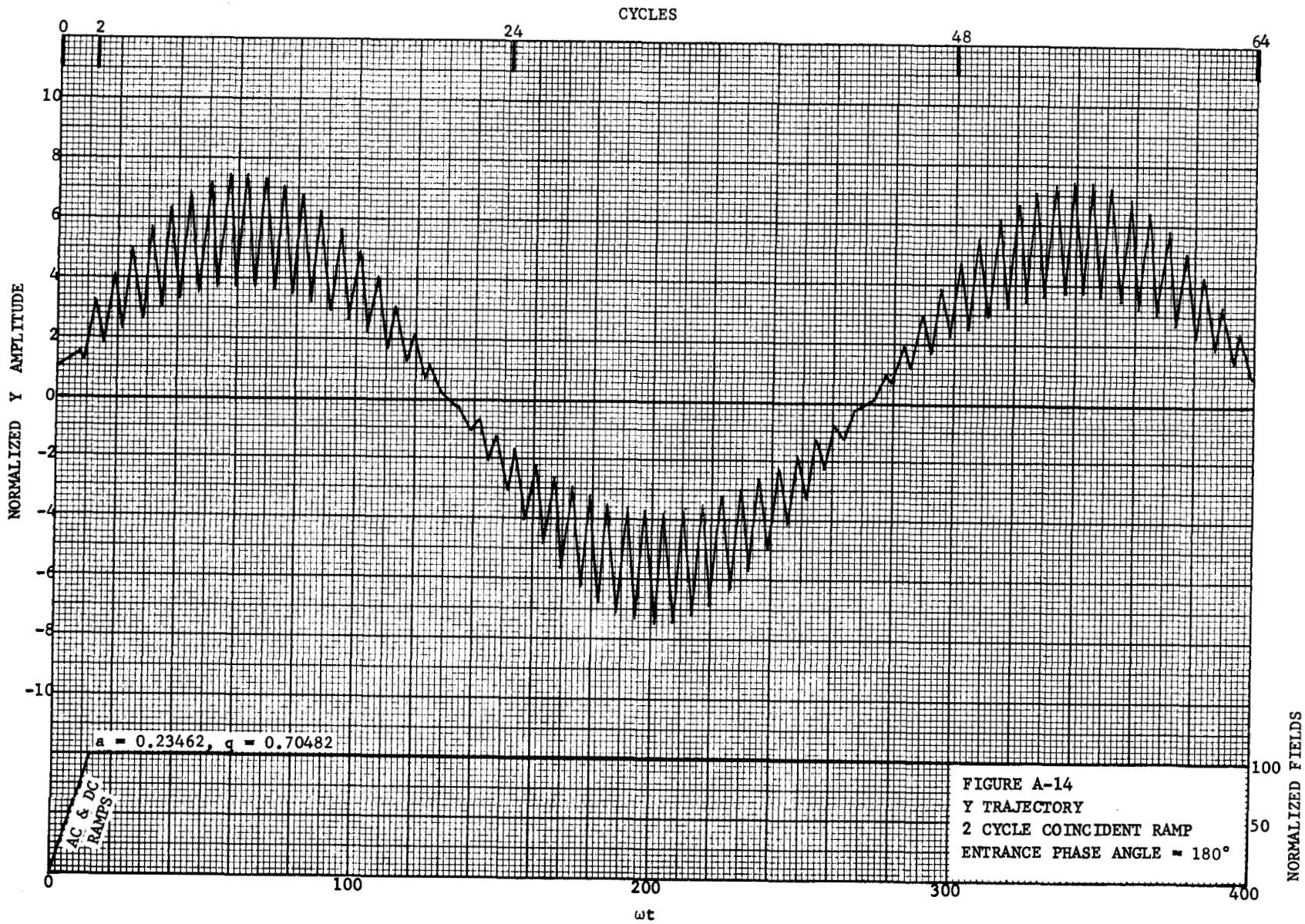

FIGURE A-14
Y TRAJECTORY
2 CYCLE COINCIDENT RAMP
ENTRANCE PHASE ANGLE = 180°

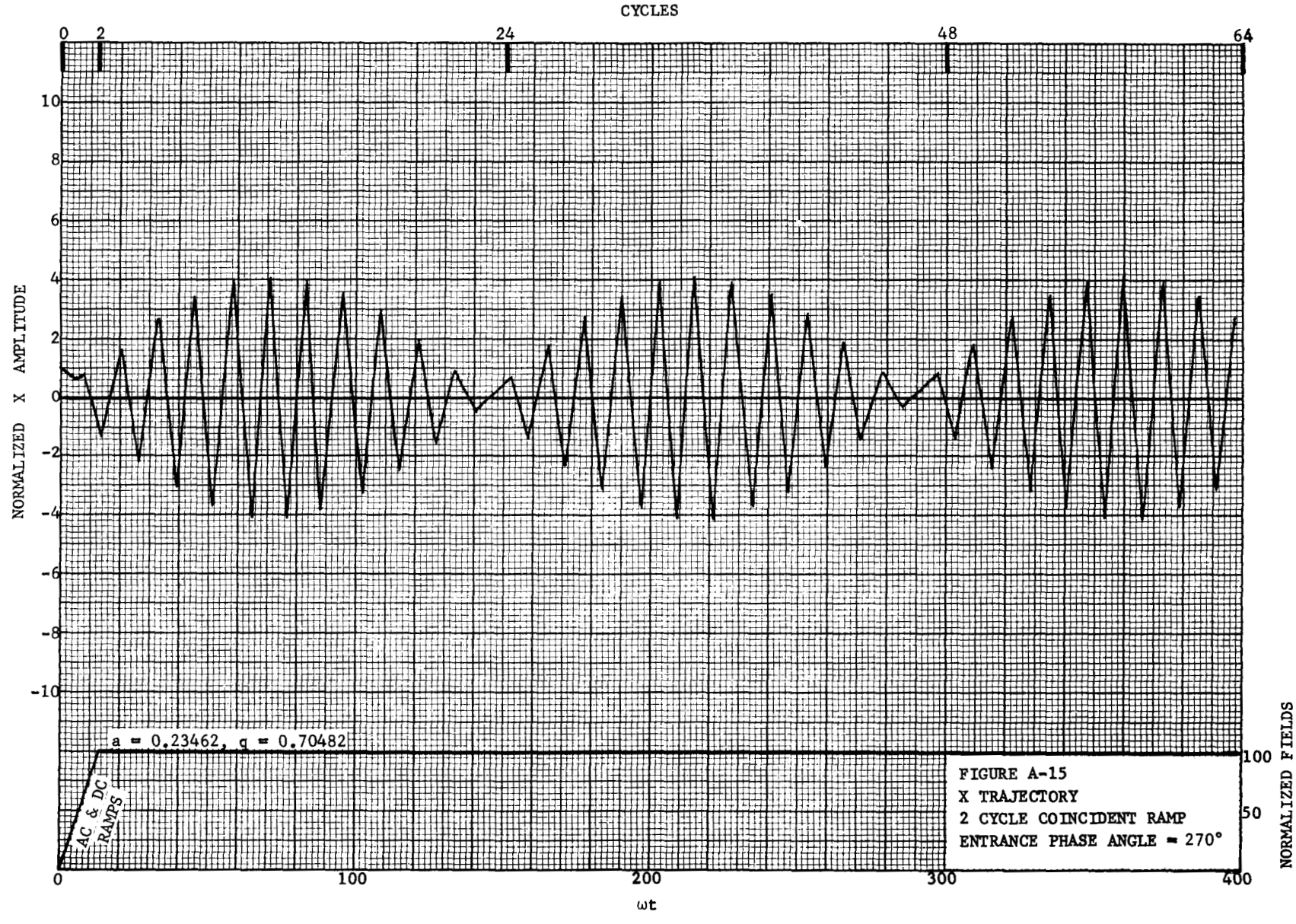

FIGURE A-15
X TRAJECTORY
2 CYCLE COINCIDENT RAMP
ENTRANCE PHASE ANGLE = 270°

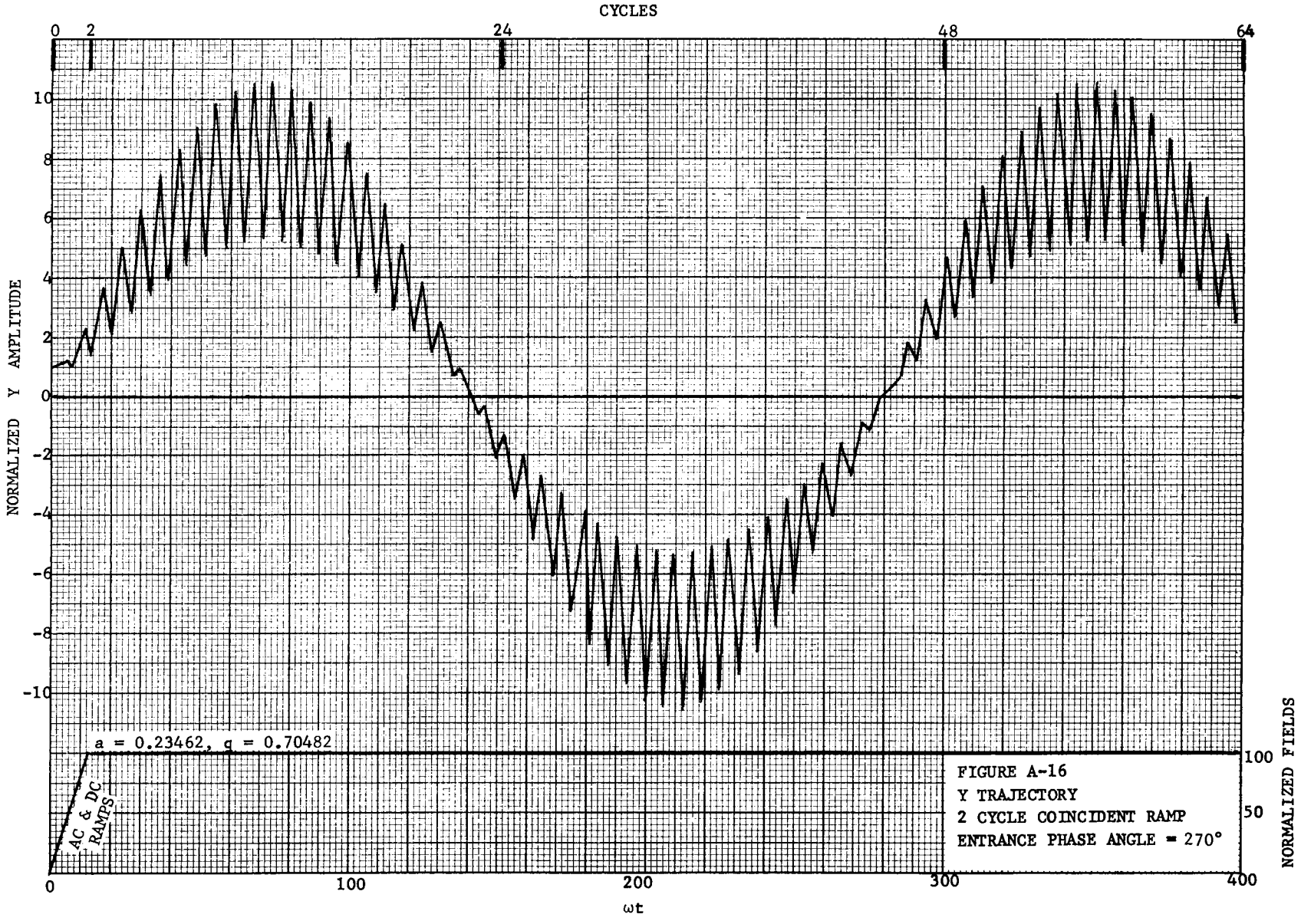

FIGURE A-16
Y TRAJECTORY
2 CYCLE COINCIDENT RAMP
ENTRANCE PHASE ANGLE = 270°

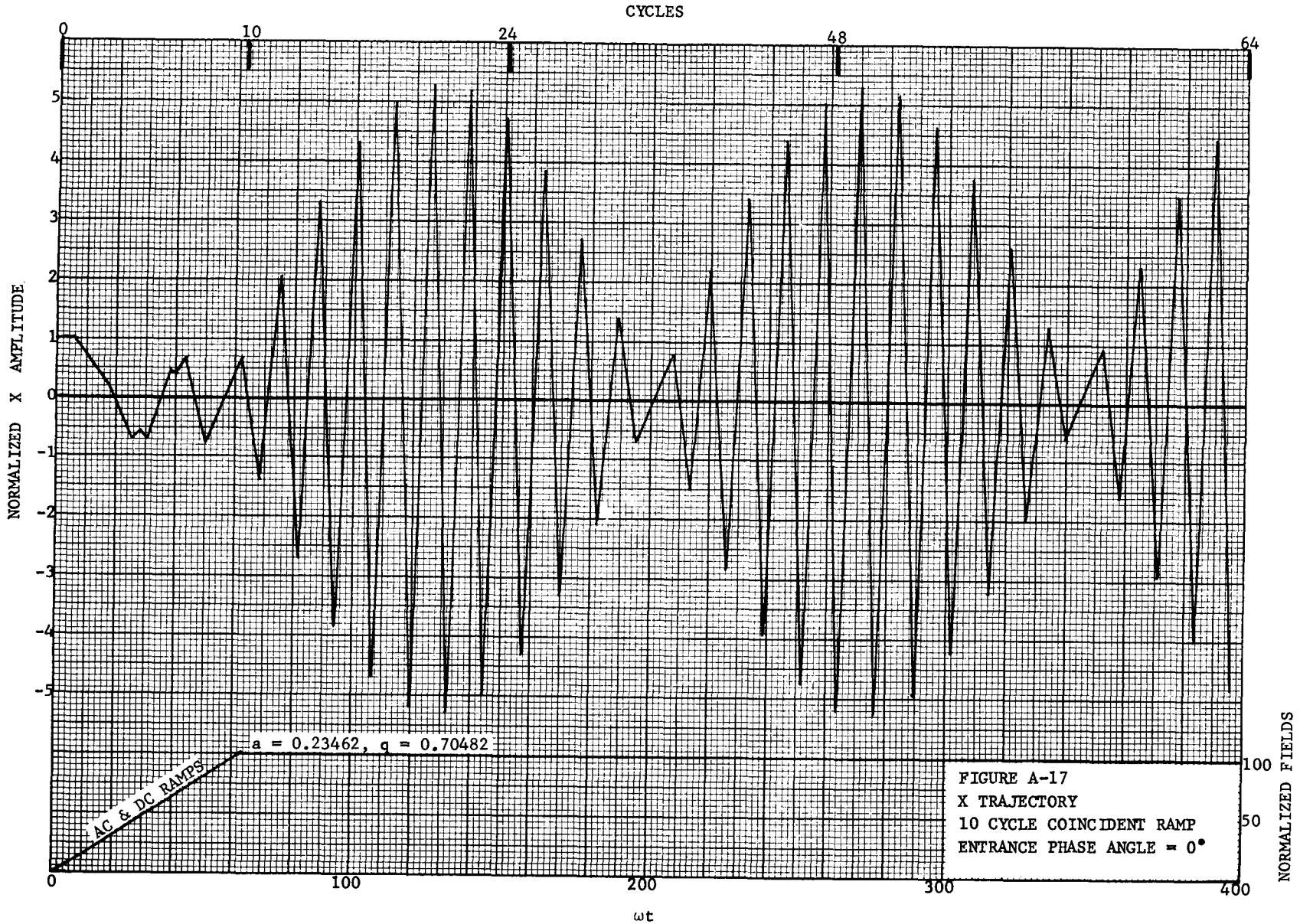

FIGURE A-17
X TRAJECTORY
10 CYCLE COINCIDENT RAMP
ENTRANCE PHASE ANGLE = 0°

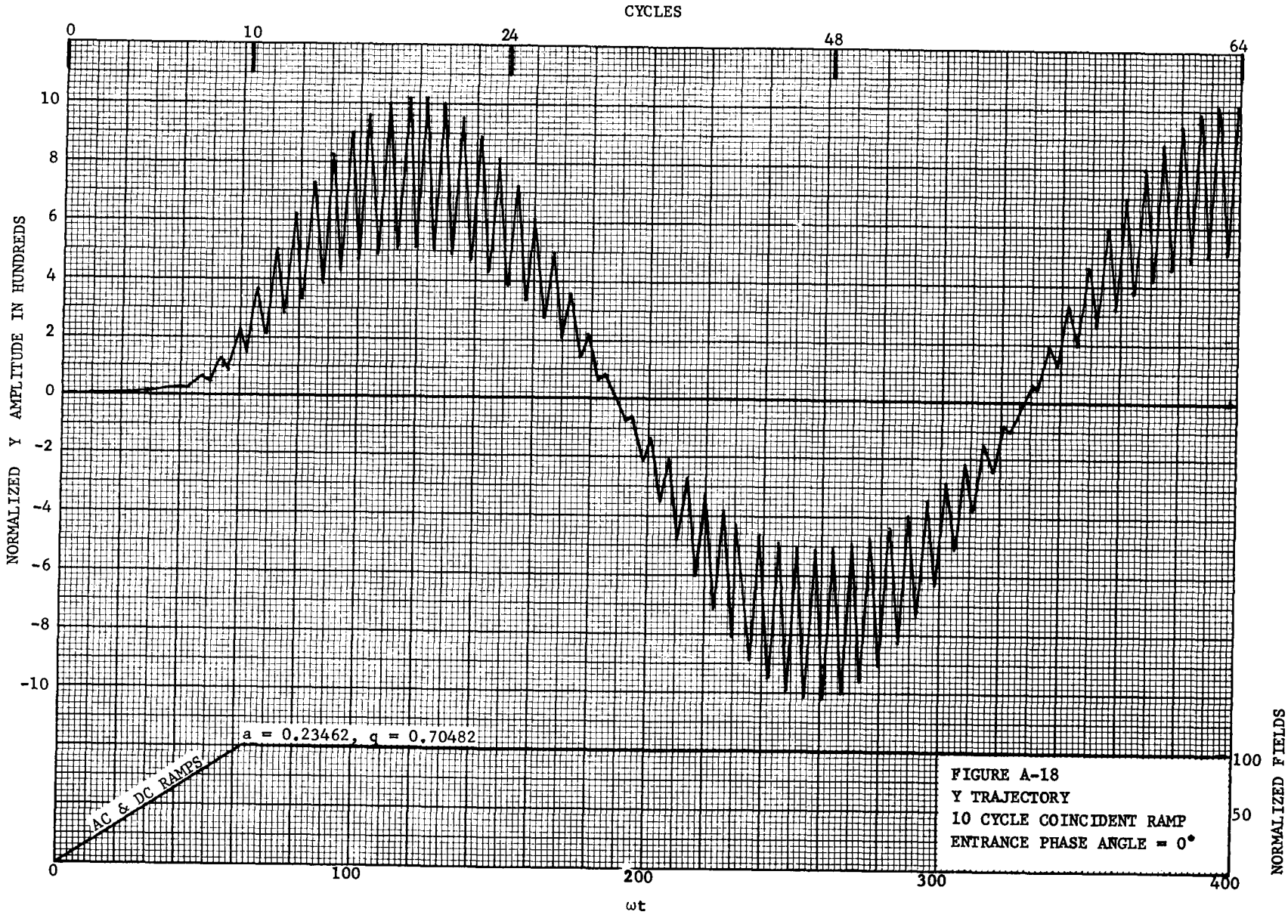

FIGURE A-18
Y TRAJECTORY
10 CYCLE COINCIDENT RAMP
ENTRANCE PHASE ANGLE = 0°

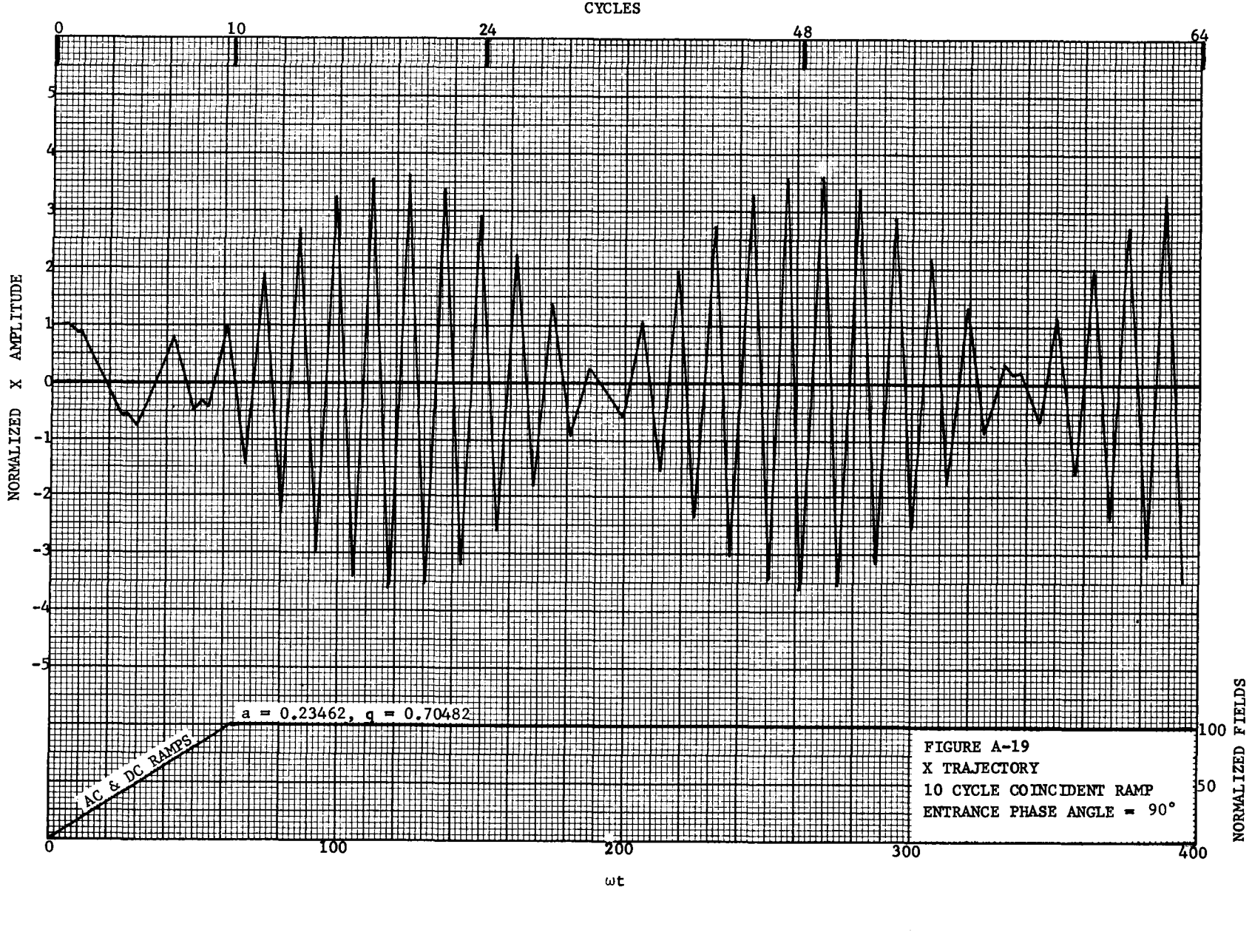

FIGURE A-19
X TRAJECTORY
10 CYCLE COINCIDENT RAMP
ENTRANCE PHASE ANGLE = 90°

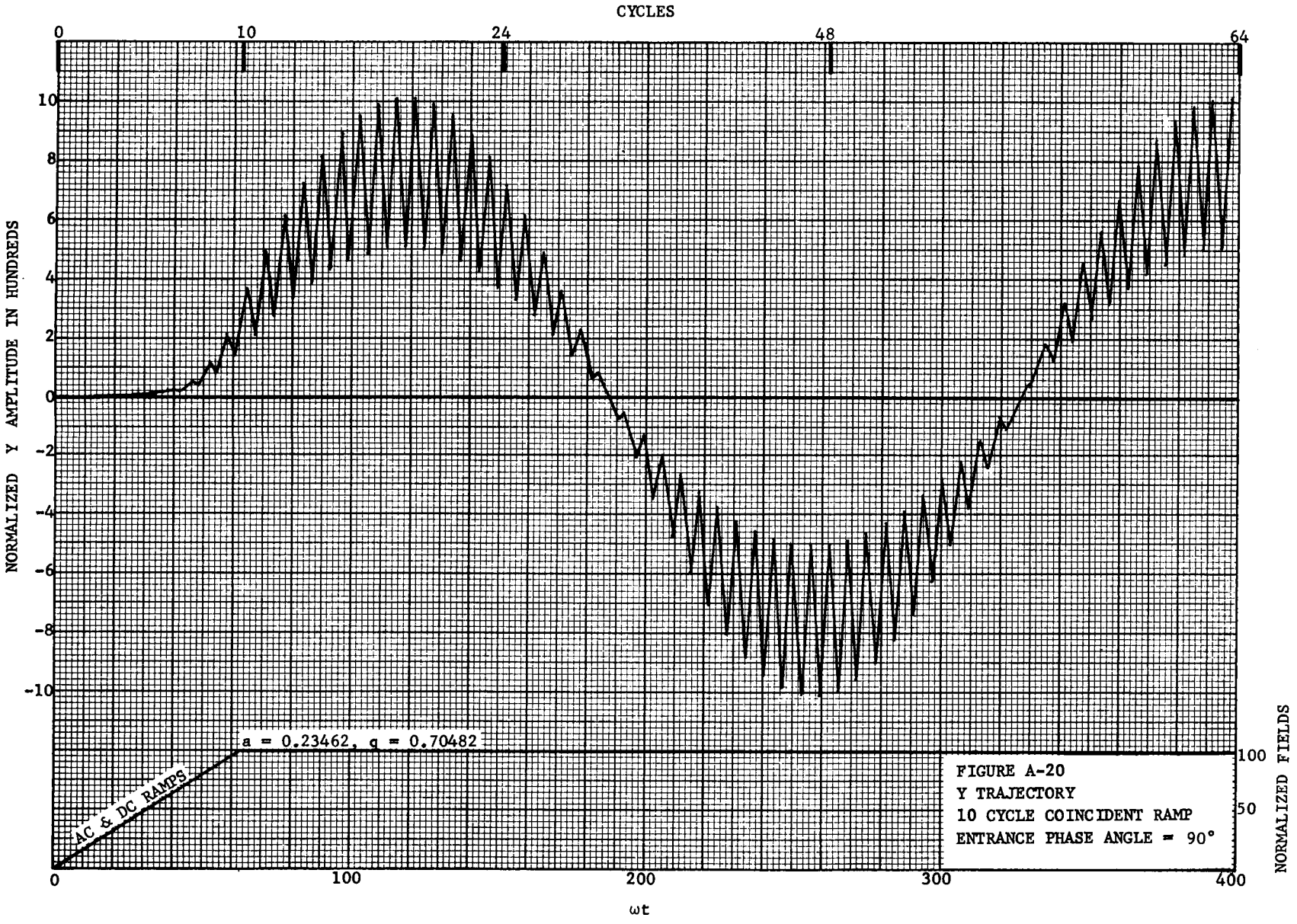

FIGURE A-20
Y TRAJECTORY
10 CYCLE COINCIDENT RAMP
ENTRANCE PHASE ANGLE = 90°

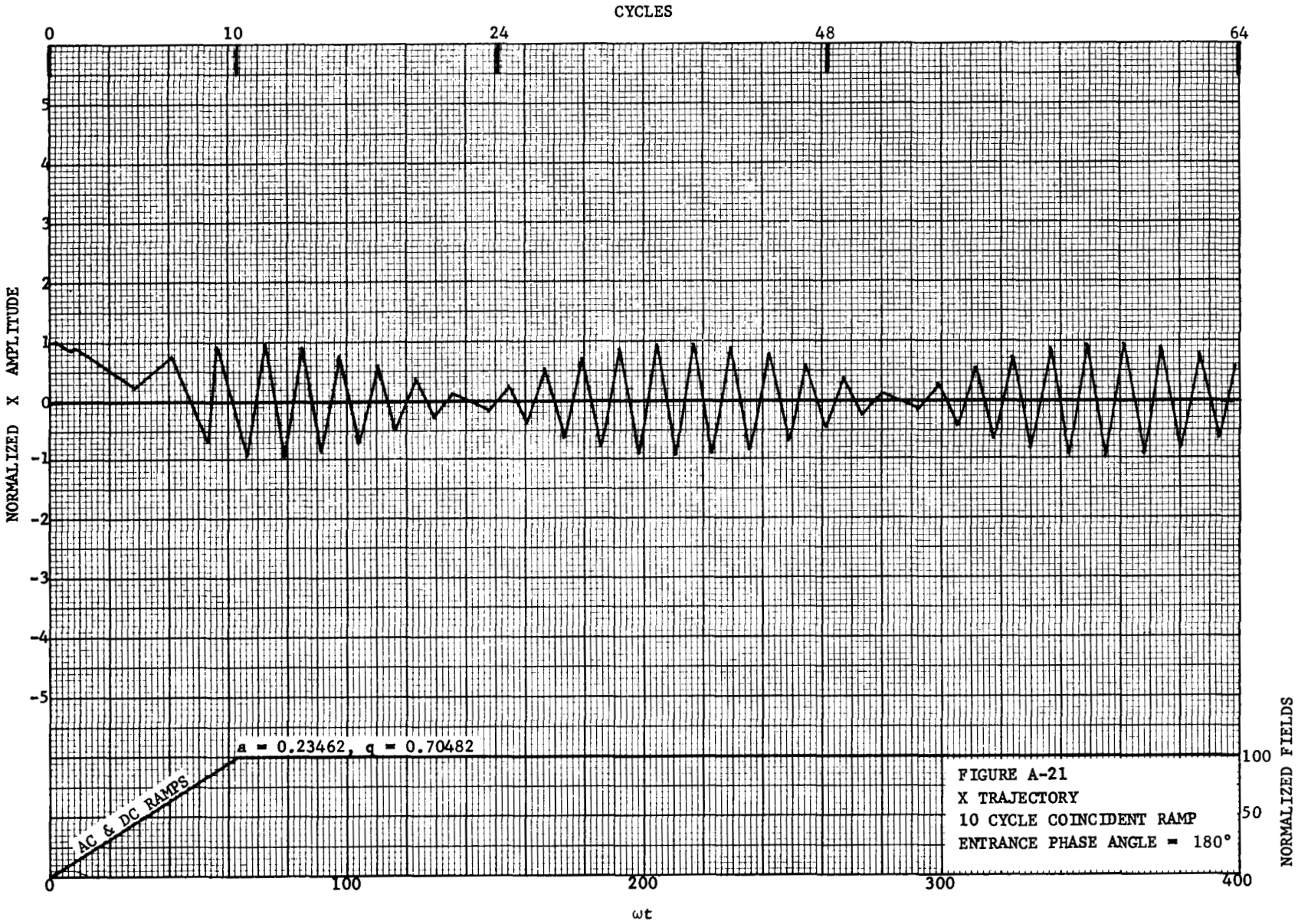

FIGURE A-21
X TRAJECTORY
10 CYCLE COINCIDENT RAMP
ENTRANCE PHASE ANGLE = 180°

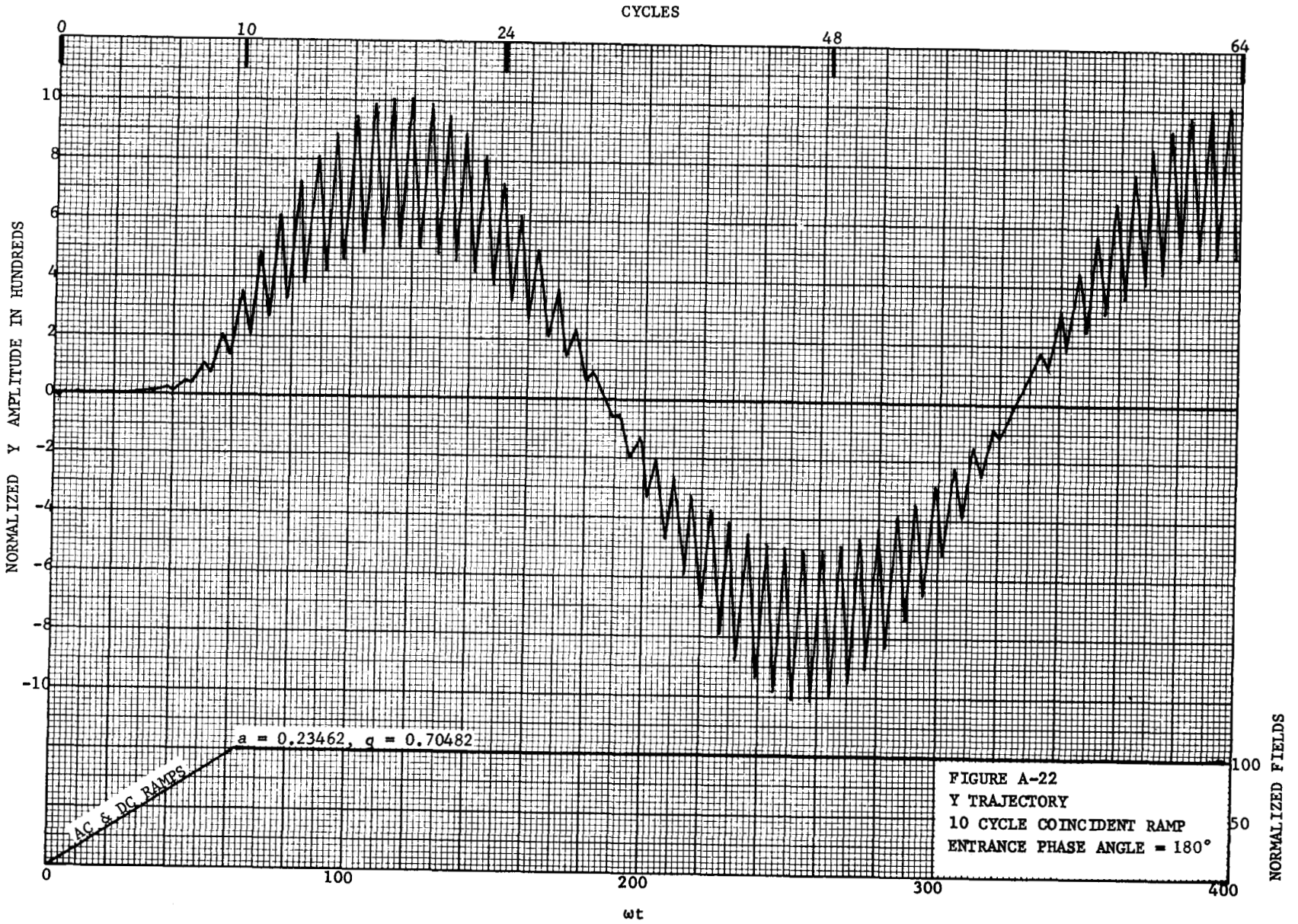
CYCLES
0
10
24
48
64
NORMALIZED Y AMPLITUDE IN HUNDREDS
10
8
6
4
2
0
-2
-4
-6
-8
-10
a = 0.23462, q = 0.70482
AC & DC RAMPS
0
100
200
300
400
ωt
100
50
NORMALIZED FIELDS
FIGURE A-22
Y TRAJECTORY
10 CYCLE COINCIDENT RAMP
ENTRANCE PHASE ANGLE = 180°

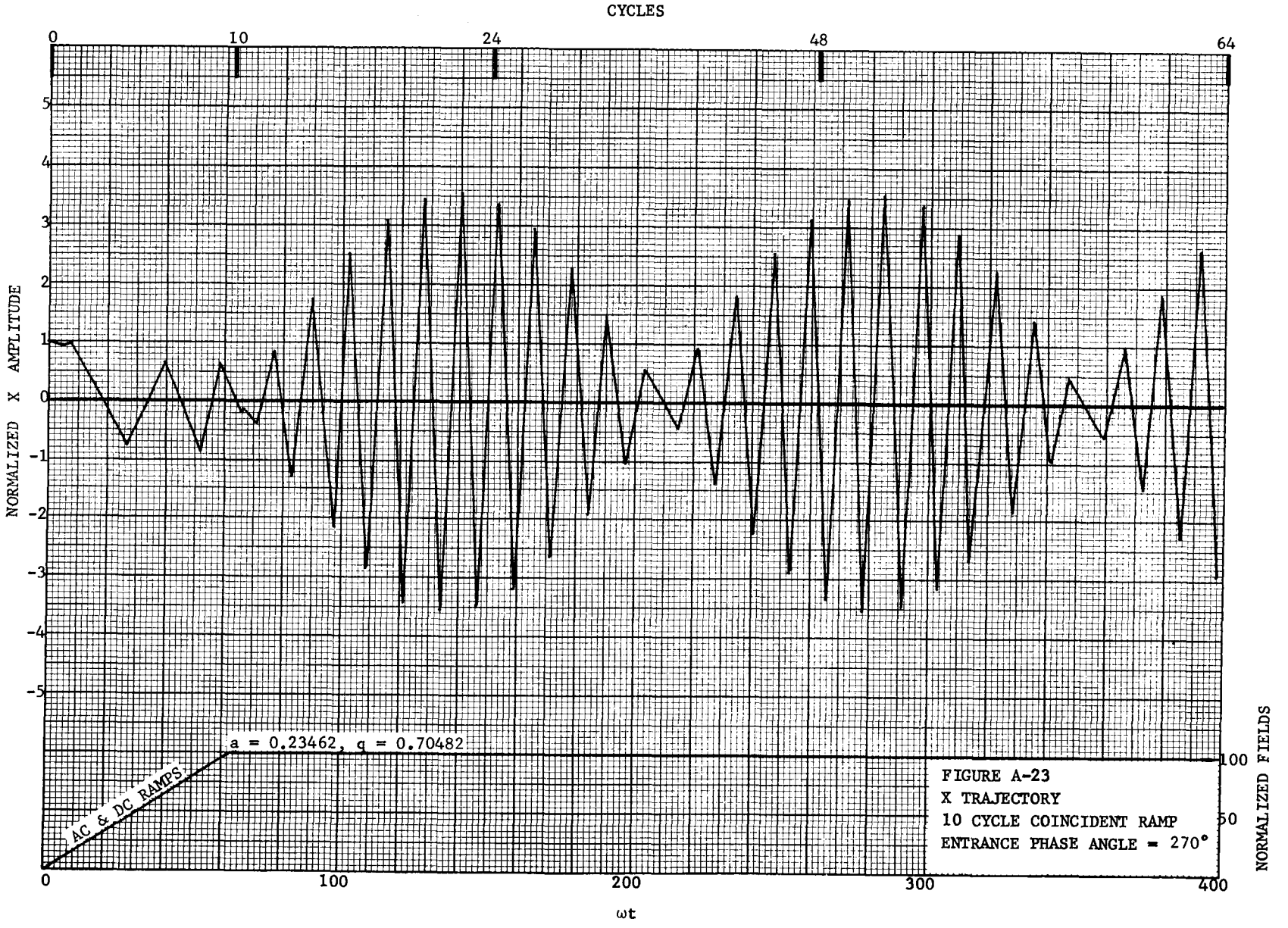

FIGURE A-23
X TRAJECTORY
10 CYCLE COINCIDENT RAMP
ENTRANCE PHASE ANGLE = 270°

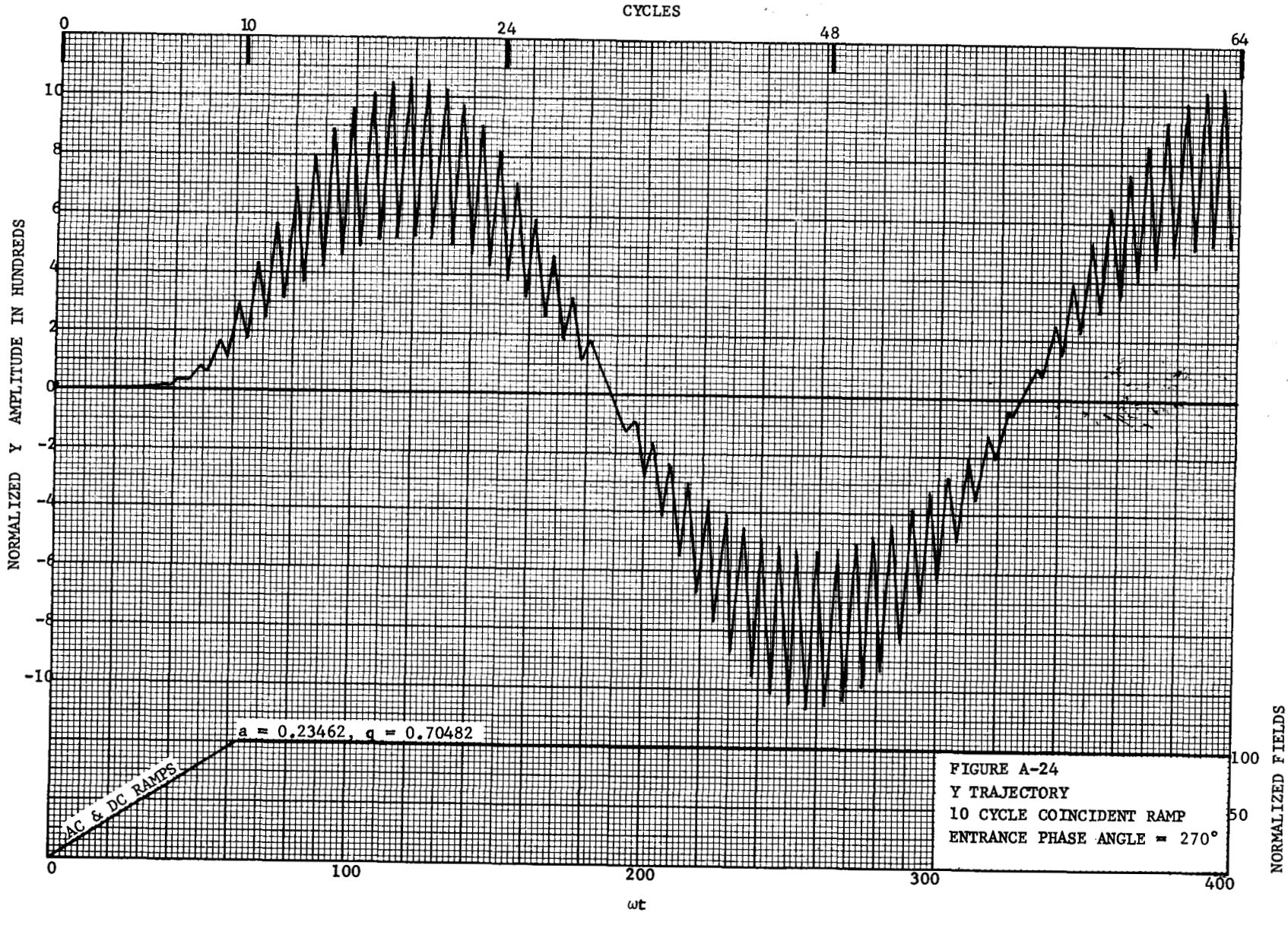

FIGURE A-24
Y TRAJECTORY
10 CYCLE COINCIDENT RAMP
ENTRANCE PHASE ANGLE = 270°

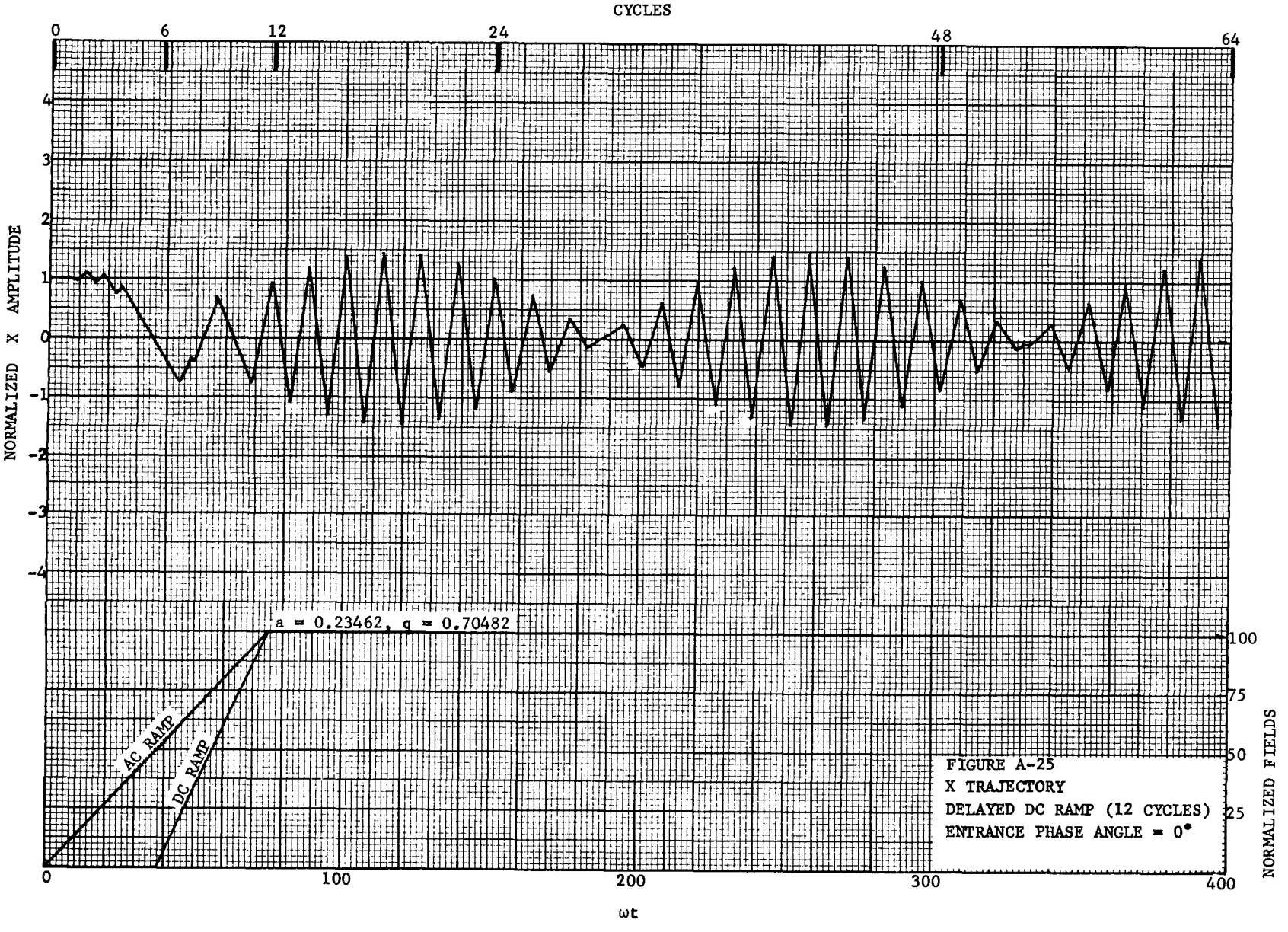

FIGURE A-25
X TRAJECTORY
DELAYED DC RAMP (12 CYCLES)
ENTRANCE PHASE ANGLE = 0°

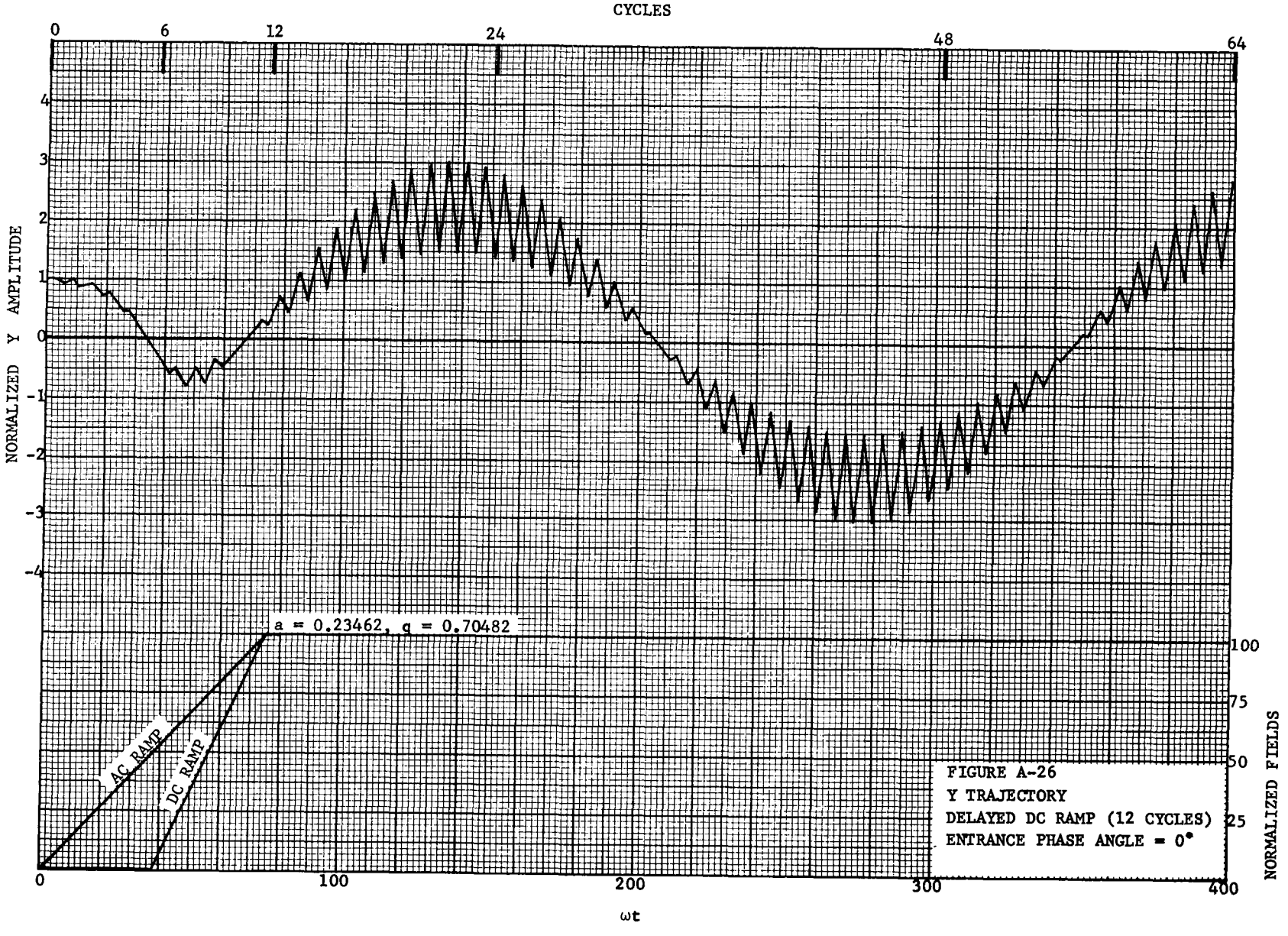

FIGURE A-26
Y TRAJECTORY
DELAYED DC RAMP (12 CYCLES)
ENTRANCE PHASE ANGLE = 0°

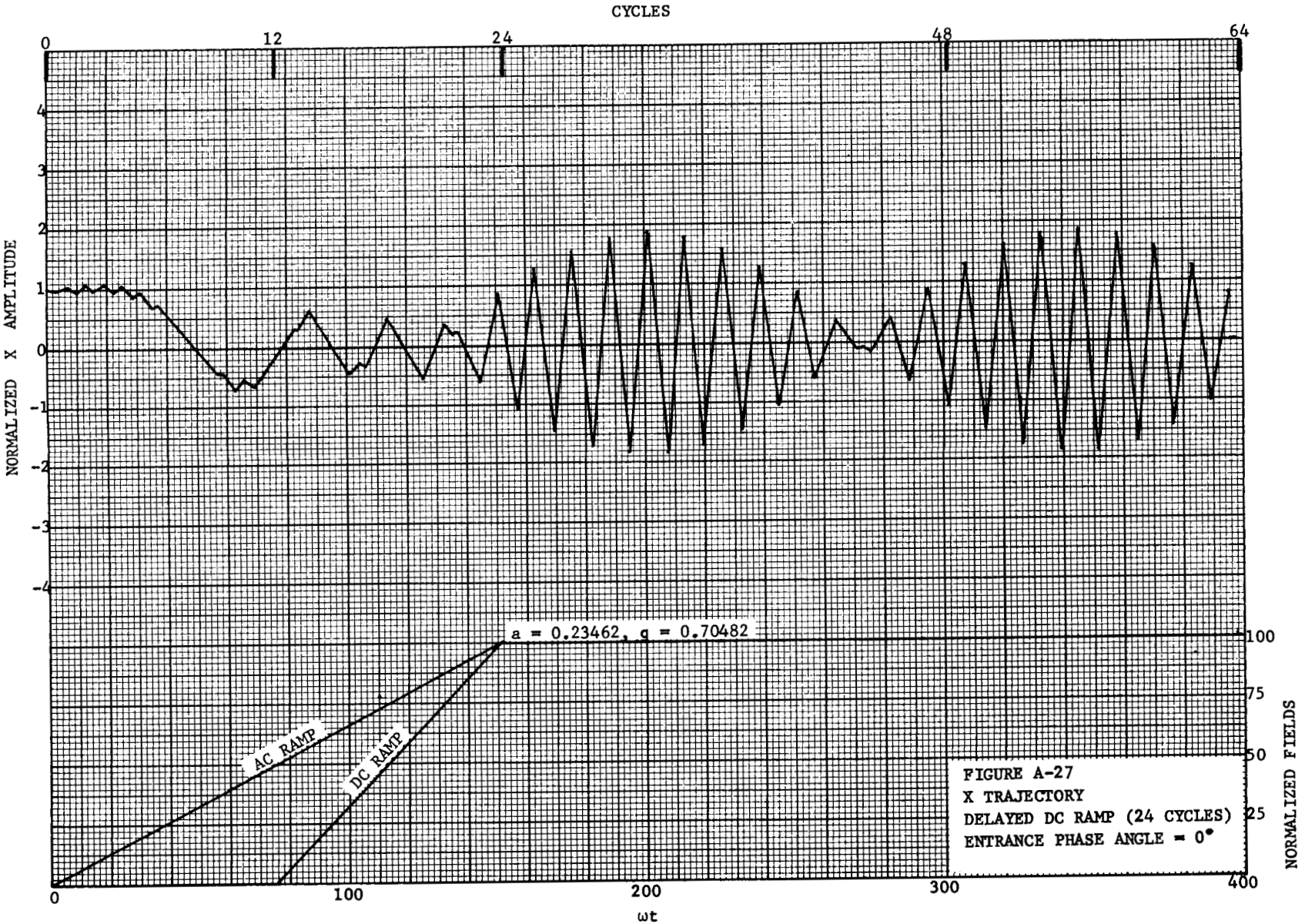

FIGURE A-27
X TRAJECTORY
DELAYED DC RAMP (24 CYCLES)
ENTRANCE PHASE ANGLE = 0°

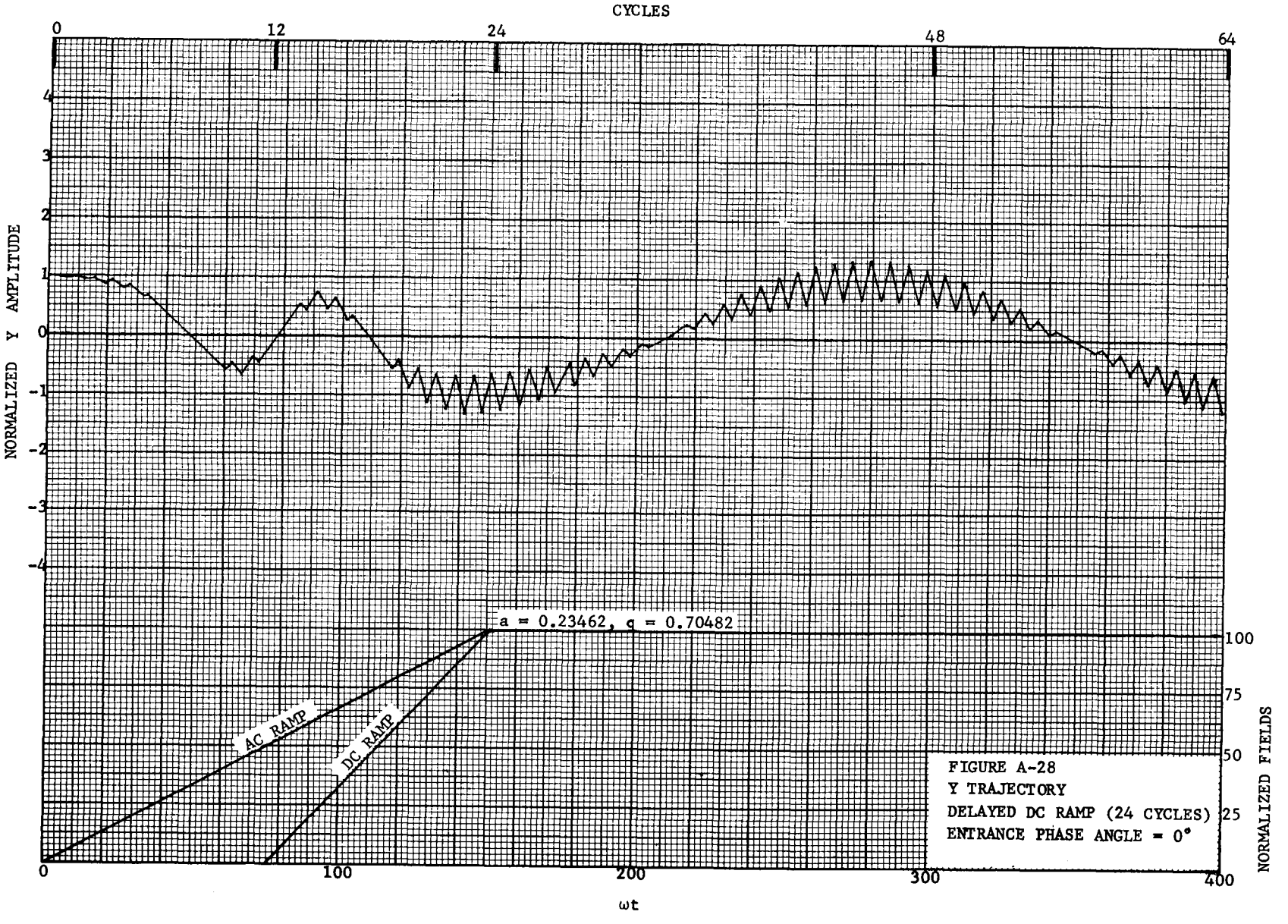

FIGURE A-28
Y TRAJECTORY
DELAYED DC RAMP (24 CYCLES)
ENTRANCE PHASE ANGLE = 0°

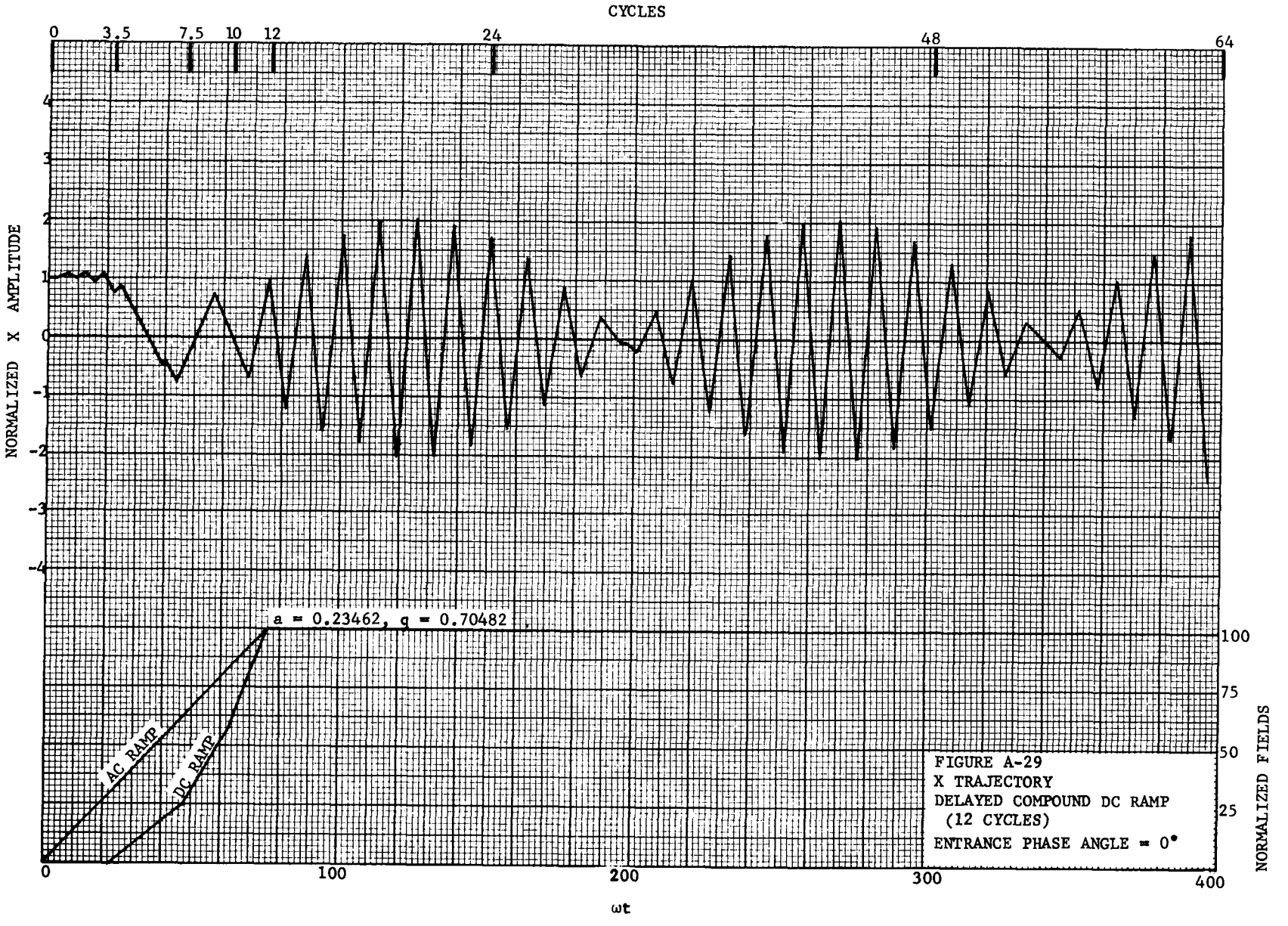

FIGURE A-29
X TRAJECTORY
DELAYED COMPOUND DC RAMP
(12 CYCLES)
ENTRANCE PHASE ANGLE = 0°

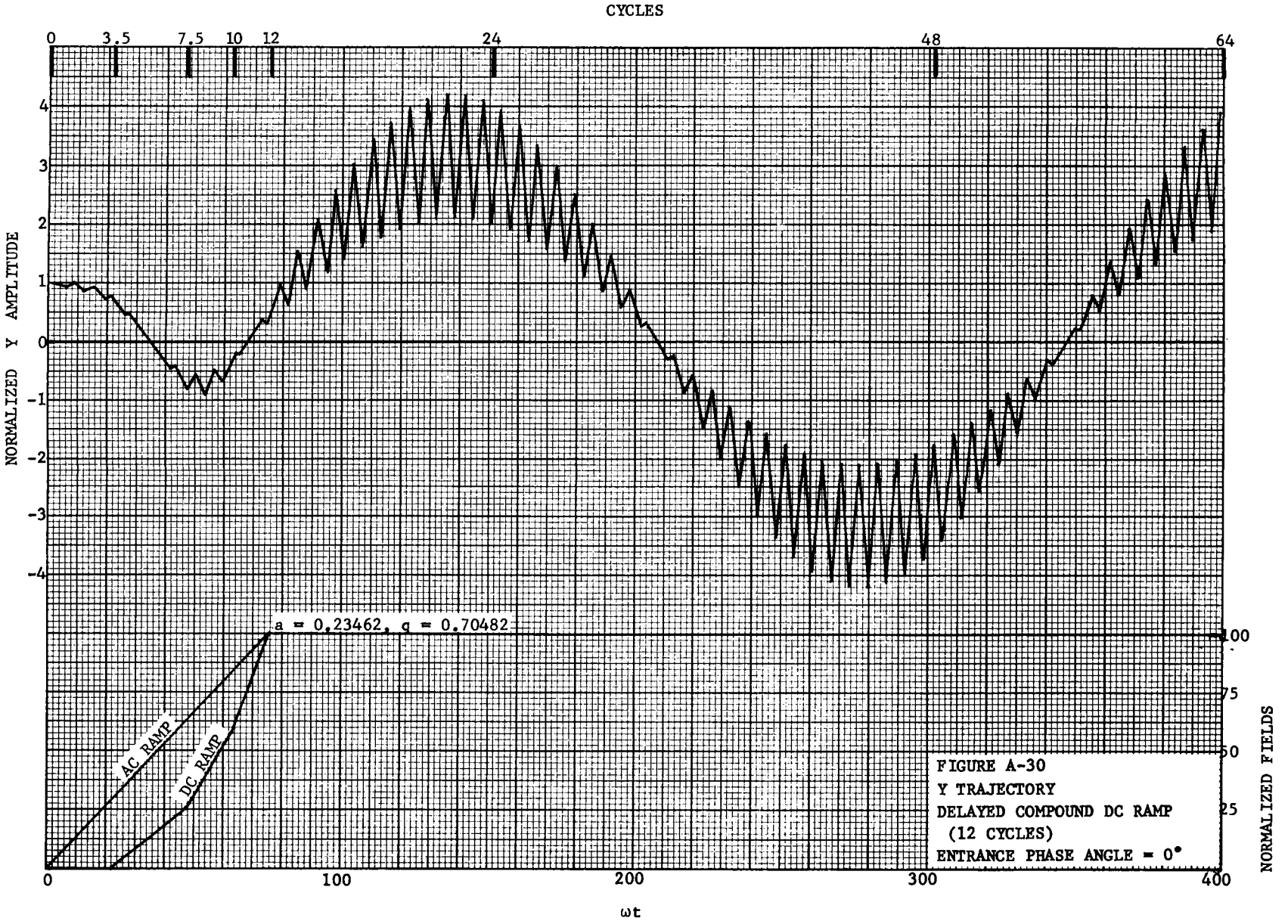

FIGURE A-30
Y TRAJECTORY
DELAYED COMPOUND DC RAMP
(12 CYCLES)
ENTRANCE PHASE ANGLE = 0°

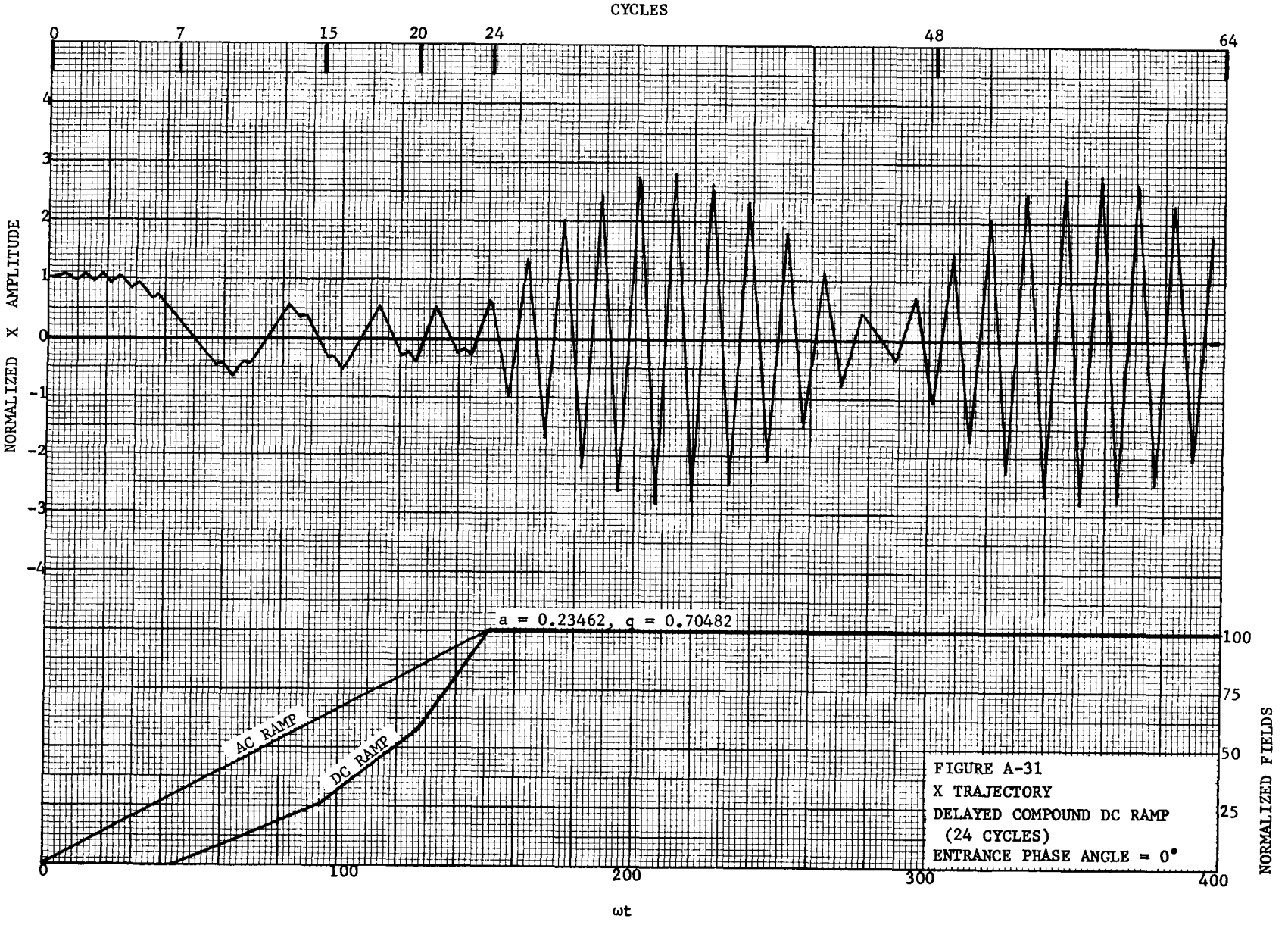

FIGURE A-31
X TRAJECTORY
DELAYED COMPOUND DC RAMP
(24 CYCLES)
ENTRANCE PHASE ANGLE = 0°

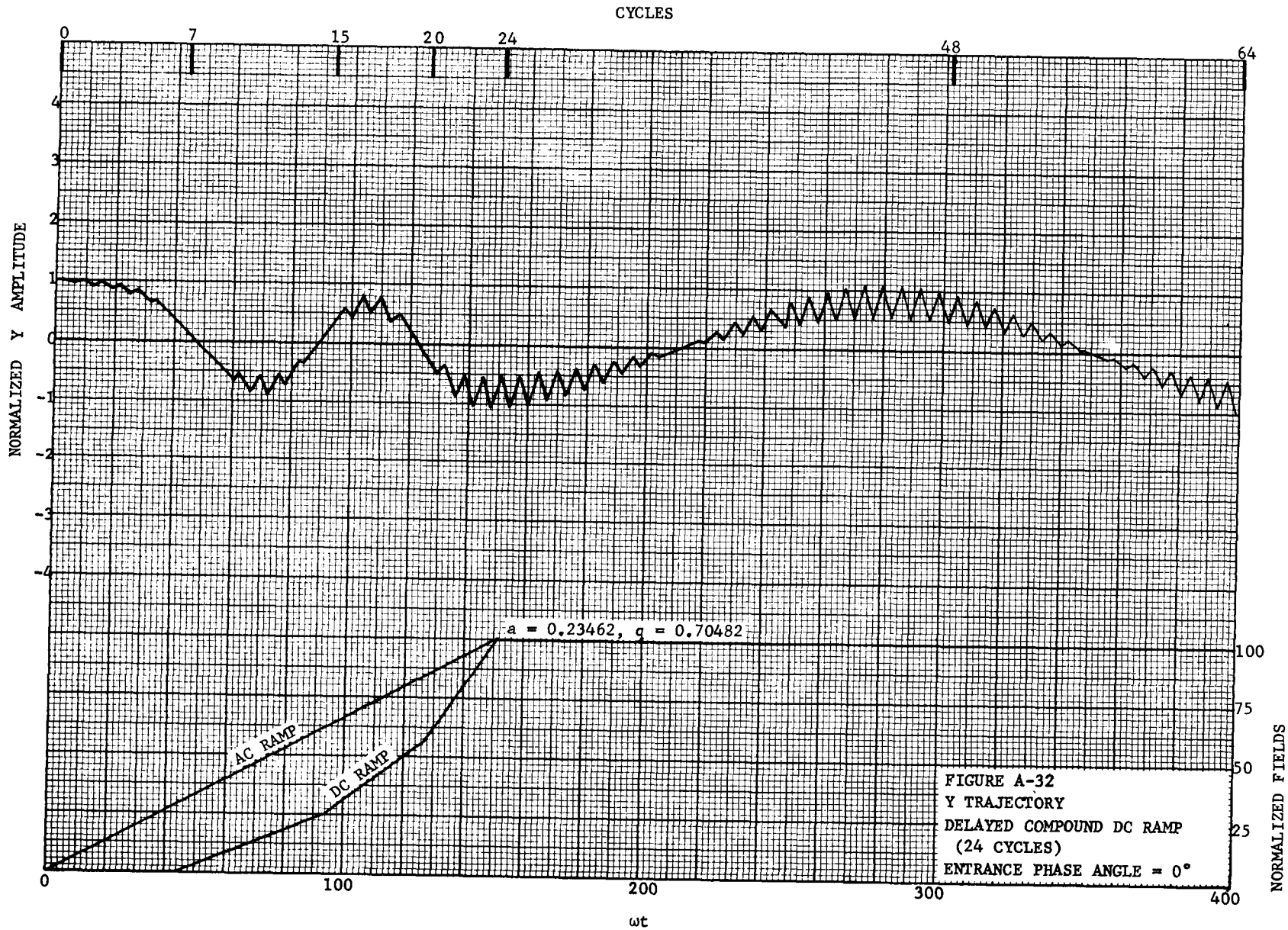

FIGURE A-32
Y TRAJECTORY
DELAYED COMPOUND DC RAMP
(24 CYCLES)
ENTRANCE PHASE ANGLE = 0°

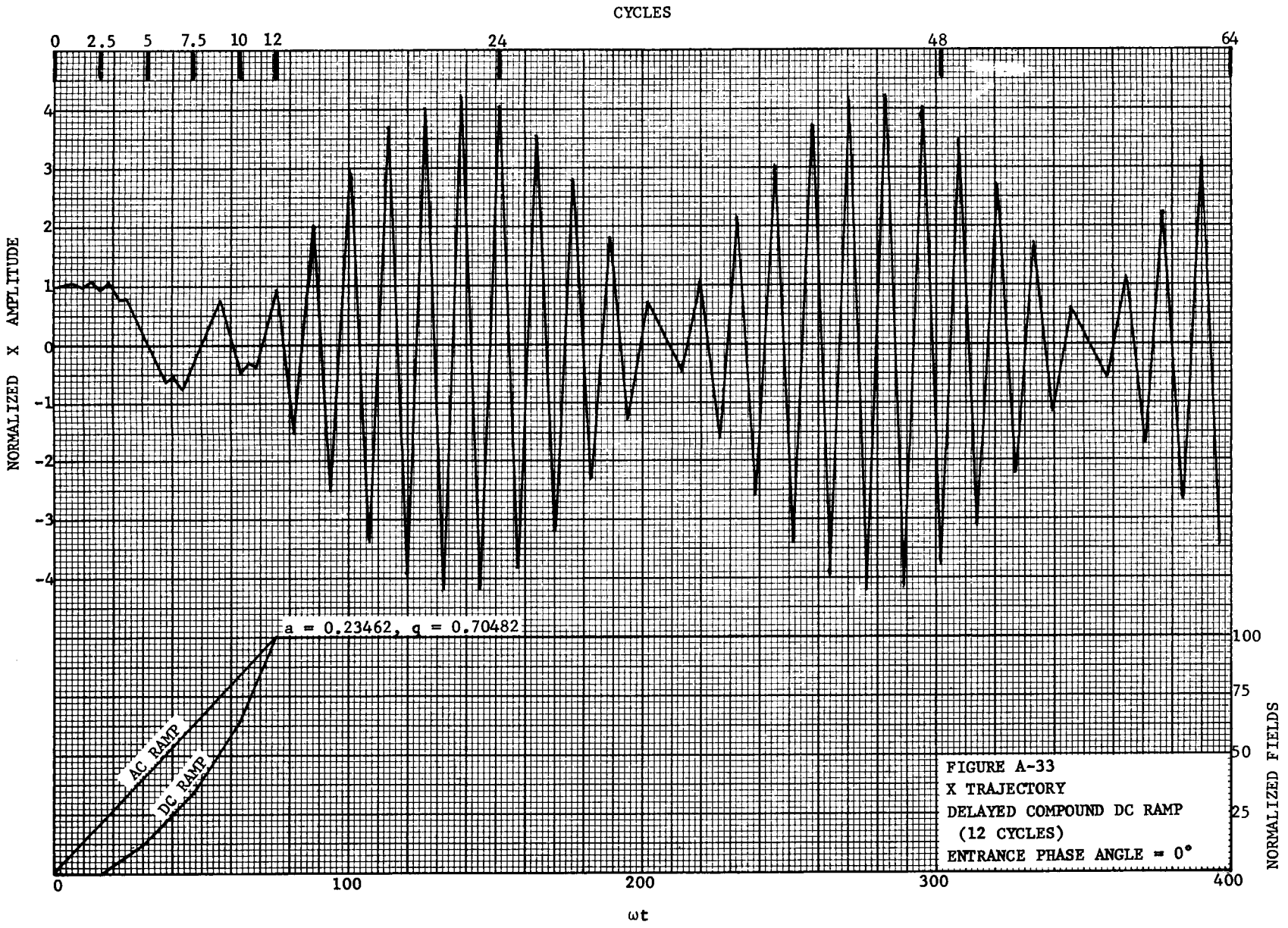

FIGURE A-33
X TRAJECTORY
DELAYED COMPOUND DC RAMP
(12 CYCLES)
ENTRANCE PHASE ANGLE = 0°

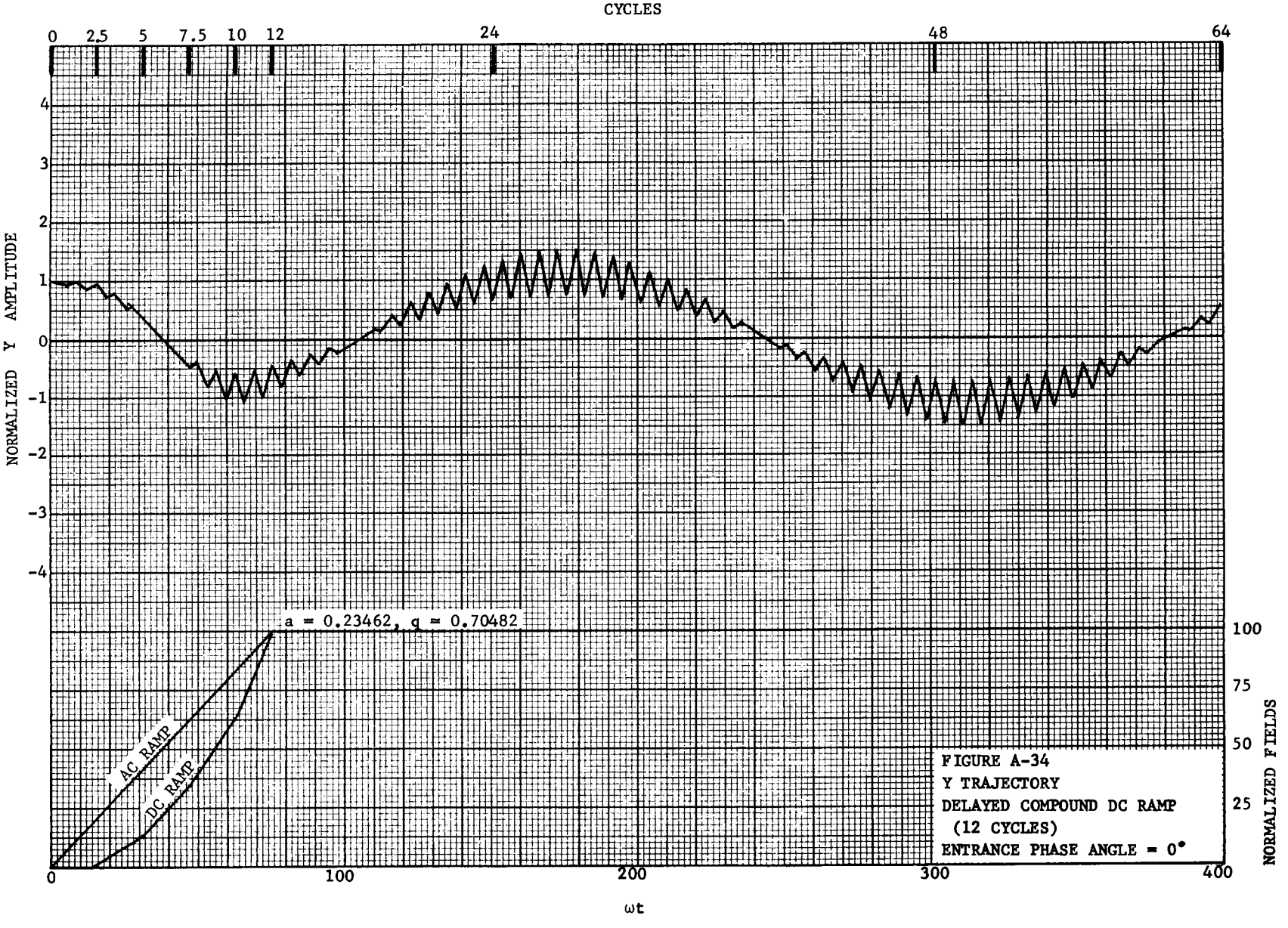

FIGURE A-34
Y TRAJECTORY
DELAYED COMPOUND DC RAMP
(12 CYCLES)
ENTRANCE PHASE ANGLE = 0°

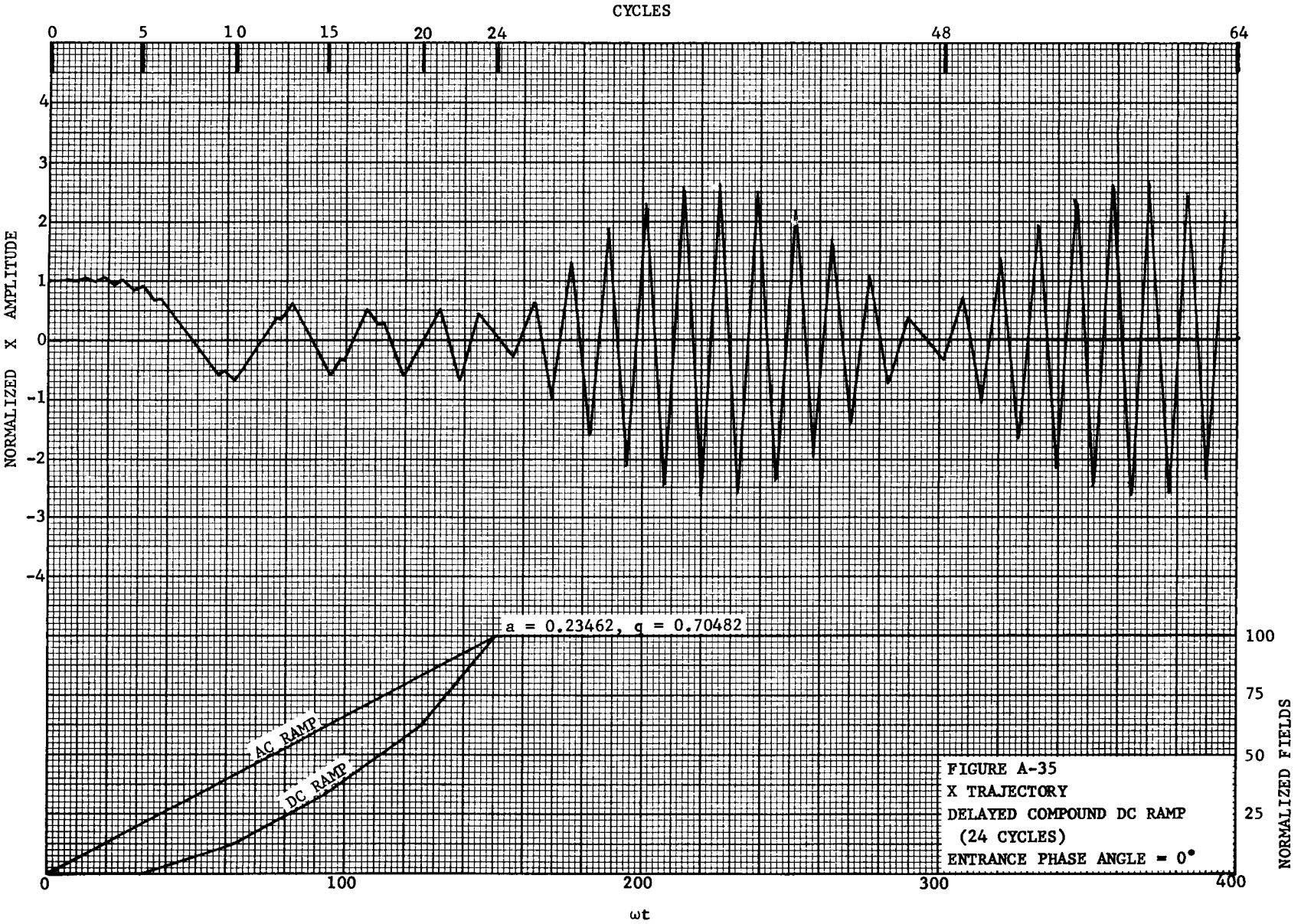

FIGURE A-35
X TRAJECTORY
DELAYED COMPOUND DC RAMP
(24 CYCLES)
ENTRANCE PHASE ANGLE = 0°

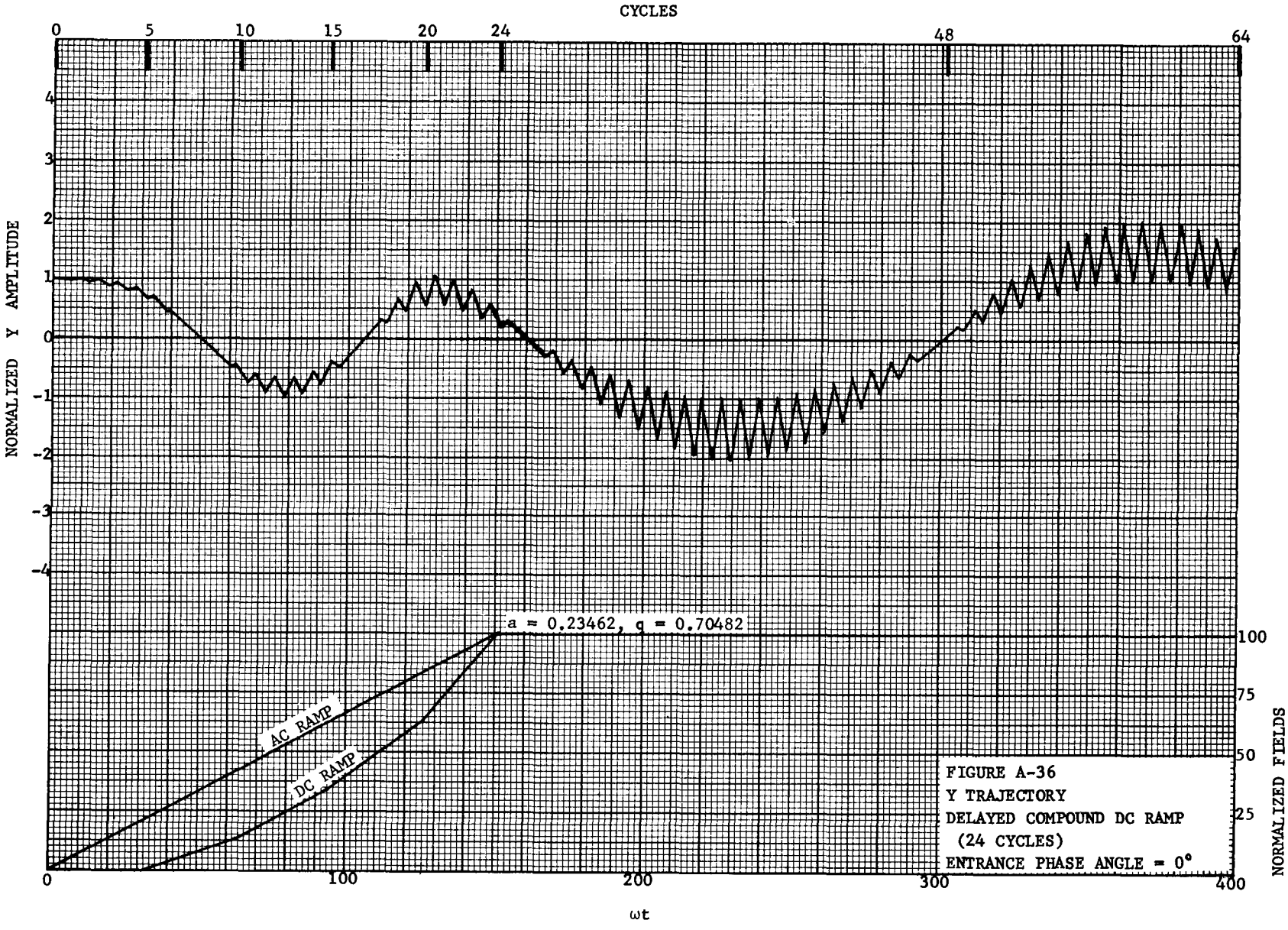

FIGURE A-36
Y TRAJECTORY
DELAYED COMPOUND DC RAMP
(24 CYCLES)
ENTRANCE PHASE ANGLE = 0°